CANCER

The Rho Exchange Factors Vav2 and Vav3 Control a Lung Metastasis–Specific Transcriptional Program in Breast Cancer Cells

Carmen Citterio,[1,2]* Mauricio Menacho-Márquez,[1,2]* Ramón García-Escudero,[3] Romain M. Larive,[1,2] Olga Barreiro,[4] Francisco Sánchez-Madrid,[4] Jesús M. Paramio,[3] Xosé R. Bustelo[1,2]†

The guanosine triphosphatases of the Rho and Rac subfamilies regulate protumorigenic pathways and are activated by guanine nucleotide exchange factors (Rho GEFs), which could be potential targets for anticancer therapies. We report that two Rho GEFs, Vav2 and Vav3, play synergistic roles in breast cancer by sustaining tumor growth, neoangiogenesis, and many of the steps involved in lung-specific metastasis. The involvement of Vav proteins in these processes did not correlate with Rac1 and RhoA activity or cell migration, implying the presence of additional biological programs. Microarray analyses revealed that Vav2 and Vav3 controlled a vast transcriptional program in breast cancer cells through mechanisms that were shared between the two proteins, isoform-specific or synergistic. Furthermore, the abundance of Vav-regulated transcripts was modulated by Rac1-dependent and Rac1-independent pathways. This transcriptome encoded therapeutically targetable proteins that played nonredundant roles in primary tumorigenesis and lung-specific metastasis, such as integrin-linked kinase (Ilk), the transforming growth factor–β family ligand inhibin βA, cyclooxygenase-2, and the epithelial cell adhesion molecule Tacstd2. It also contained gene signatures that predicted disease outcome in breast cancer patients. These results identify possible targets for treating breast cancer and lung metastases and provide a potential diagnostic tool for clinical use.

INTRODUCTION

The guanosine triphosphatases (GTPases) Rho and Rac (Rho) and their proximal effectors frequently show increased abundance in tumors, where they regulate biological functions that favor the proliferation, apoptosis, invasion, metastasis, or resistance of cancer cells to anticancer treatments. This has led to the idea that they could be potential antitumoral and antimetastatic targets (*1*). Because Rho proteins are not mutated in tumors (*1*), a possible means of inhibiting the signal transduction pathways that they mediate is to block the upstream guanine nucleotide exchange factors (GEFs). These enzymes catalyze the exchange of guanosine diphosphate (GDP) by GTP on Rho proteins, thereby favoring their rapid transition from their inactive (GDP-bound) to their active (GTP-bound) states during cell signaling (*2*, *3*). Knockout mice and knockdown cells have demonstrated that eliminating individual Rho GEFs can impair the growth of skin cancer [T cell lymphoma invasion and metastasis-inducing protein 1 (Tiam1)] (*4*), chronic myelogenous leukemia subtypes (Vav3) (*5*), colorectal cancer [Tiam1, adenomatous polyposis coli–stimulated exchange factor 1 (Asef1, also known as ArhGEF4), and Asef2] (*6*, *7*), and breast cancer [phosphatidylinositol 3,4,5-trisphosphate–dependent Rac exchanger 1 (P-Rex1) and P-Rex2] (*8*, *9*). In addition, inhibitors that block the interaction of a subset of GEFs with Rac1 can block chronic myelogenous leukemia in animal models (*10*). The role of Rho GEFs in metastasis is not as well characterized, although current evidence indicates that some Rac1 GEFs play either antimetastatic (Tiam1) (*11*) or prometastatic (P-Rex1) (*12*) roles in different tumor types.

[1]Centro de Investigación del Cáncer, CSIC-University of Salamanca, 37007 Salamanca, Spain. [2]Instituto de Biología Molecular y Celular del Cáncer, CSIC-University of Salamanca, 37007 Salamanca, Spain. [3]Molecular Oncology Unit, CIEMAT, 28040 Madrid, Spain. [4]Centro Nacional de Investigaciones Cardiovasculares, 28029 Madrid, Spain.
*These authors contributed equally to this work.
†To whom correspondence should be addressed. E-mail: xbustelo@usal.es

However, the identification of the good GEF targets in different cancer and metastatic settings is complicated by various hurdles, one of which is the size of the Rho GEF family, which in humans is composed of 65 members (*2*, *3*). Although they share either catalytic Dbl-homology (DH, 54 members) or dedicator of cytokinesis (Dock) homology region 2 (DHR2, 11 members) domains, they differ widely in terms of ancillary domains and tissue distribution patterns. Thus, even GEFs with the same catalytic specificity can stimulate the downstream GTPase only in specific cell types, stimulation conditions, or subcellular localizations (*2*, *3*). In addition, their noncatalytic domains can limit the spectrum of effectors engaged by the stimulated GTPases (*13*–*15*) and activate GTPase-independent routes (*9*, *16*–*18*). The type of oncogenic events present in tumors adds another layer of complexity because different oncoproteins may restrict the spectrum of Rho GEFs that could be preferentially activated in a particular tumor (*8*, *9*). For example, tumors with constitutively active phosphatidylinositol 3-kinase are expected to preferentially activate phosphatidylinositol 3,4,5-trisphosphate–dependent Rho GEFs such as P-Rex1 and P-Rex2. These observations indicate that the identification of therapeutically relevant Rho GEFs requires the identification of those specifically enriched or activated in tumors, the determination of the functional redundancies among them, and the dissection of the GEF-dependent and GEF-independent biological processes that affect cancer growth or metastasis in vivo.

Here, we sought to tackle those issues in the case of Vav proteins, a specific regulatory subgroup of the DH family (*19*). These proteins epitomize the complexity existing in the Rho GEF world. Vertebrate species have three members (Vav1, Vav2, and Vav3) with overlapping, but not identical, cellular and tissues distributions. In addition, these proteins contain highly similar and complex structures that encompass regulatory, catalytic, catalytic-associated, and adaptor domains (*19*). As a consequence, they can induce cellular responses in a GTPase-dependent and GTPase-independent manner (*16*, *18*, *19*). Finally, Vav proteins constitute an idiosyncratic subclass

within the Rho GEF family because they are the only GEFs positively regulated by direct tyrosine phosphorylation during signal transduction (*19*–*22*). Here, we have used both in silico and animal model systems to (i) compare their abundance to the rest of 51 DH family GEFs in human tumors, (ii) determine whether they played specific or redundant roles in both primary tumorigenesis and the main metastatic steps, and (iii) identify nonconventional downstream targets that could mediate Vav-dependent effects on the biology of cancer cells. This approach revealed that Vav2 and Vav3 play critical and nonredundant roles in primary breast tumors and during lung-specific metastasis. We also found a Vav2/Vav3-dependent transcriptional program that helps to explain the synergistic effect of those two proteins in primary tumorigenesis and lung-specific metastasis. These results provide a holistic view of the role of a Rho GEF subfamily in the main steps involved in the metastatic dissemination of a frequently occurring tumor, reveal a new biological program that conditions the specific tropism of metastatic breast cancer cells to the lung, and, in addition, provide information about prognostic gene signatures that could be potentially relevant in this clinical setting.

RESULTS

Human breast tumors and cancer cell lines show increased abundance of Vav family transcripts

To identify tumors with enriched Vav protein abundance and investigate functional overlap with other GEFs, we used metagenomic analyses to determine the abundance of the transcripts for the 54 human DH-family GEFs in tumors. We considered that an mRNA was more abundant in a tumor when it showed at least a twofold average enrichment in abundance in that tumor compared to other cancer types and when such variation had a statistical P value of $\leq 1 \times 10^{-4}$ (see Materials and Methods). Using these cutoff parameters, we found that the *Vav3* mRNA was consistently enriched in breast cancer samples (fig. S1A) and breast cancer cell lines (fig. S1B). In this tumor type, the *Vav3* transcript was more abundant in estrogen- and progesterone receptor–positive tumors (table S1). In addition, *Vav3* was also more abundant in breast luminal A/B tumors when compared to both normal breast and other breast cancer subtypes (table S2). As expected from previous results from Kazanietz's laboratory (*8*), the metagenomic analyses also revealed that the *P-Rex1* mRNA was enriched in breast cancer relative to other tumor types. The enrichment in *Vav3* and *P-Rex1* transcript abundance in breast cancer samples was comparable, although not fully overlapping, to that of *ERBB2* (v-erb-b2 erythroblastic leukemia viral oncogene homolog 2) (fig. S1, C and D), a gene that is frequently overexpressed in breast cancer (*23*). The *Vav1* mRNA showed significantly greater abundance only in lymphoma-derived samples (fig. S1, A and C to E). This is probably not connected to tumor-linked requirements because *Vav1* is preferentially expressed in healthy hematopoietic cells (fig. S1F) (*19*). *Vav2* mRNA was detected in various tumor and cancer cell samples, although it did not display any statistically significant enrichment in any specific tumor type (fig. S1, C and D). It was, however, slightly enriched in abundance in breast luminal A/B tumors when compared to normal breast or other breast tumor subtypes, although the statistical significance of this variation ($P = 4.9 \times 10^{-3}$) was below our aforementioned cutoff value (table S2). The second member of the P-Rex subfamily, *P-Rex2*, showed no significant enrichment in the samples surveyed (fig. S1, C to E).

Vav proteins play critical roles in breast cancer

The above results indicated that Vav3 could play a role in breast cancer. However, the presence of other Rho GEFs that were either enriched in abundance (namely, P-Rex1) or found at basal amounts (namely, Vav2) in this tumor type called the relevance of this role into question. This question was particularly important for Vav2, a protein that shares similar regulatory properties with Vav3 (*19*). To address this issue, we first analyzed the effect of their specific knockdown in the 4T1 breast cancer cell line (*24*). These cells, which were originally isolated from a spontaneous mammary tumor in a wild-type BALB/cJ mouse, are used extensively in the breast cancer field for several reasons. First, they can grow in immunocompetent mice and are therefore still subject to the antitumorigenic and protumorigenic effects of the immune system of the host. Second, they can disseminate away from the primary tumor and metastasize in different organs of the recipient mouse. Finally, they have nonmetastatic counterparts that can be used to evaluate whether a gain of function in a particular signaling pathway can rescue specific stages of the metastatic process (*24*). In our particular case, these cells were also useful because they express both Vav2 and Vav3 (fig. S2, A and B), thereby allowing investigation into issues of functional redundancy and specificity. To clearly discern the extent of functional overlap between Vav2 and Vav3, we generated knockdown cell clones lacking Vav2, Vav3, or both proteins (table S3). In addition, we used one of the *Vav2;Vav3* knockdown cell clones to generate "rescued" cell line derivatives stably overexpressing Vav2, Vav3, Vav2 plus Vav3, constitutively active $Vav2^{Y172F}$, or catalytically inactive $Vav2^{R373A}$ (table S3). The depletion of the indicated Vav family protein was confirmed by quantitative reverse transcription polymerase chain reaction (qRT-PCR) (fig. S2, A and B). The reexpression of the appropriate Vav family member in the knockdown cells was confirmed by qRT-PCR (fig. S2, C and D) and Western blot (fig. S2, E and F) techniques. Using a GTPase-linked immunosorbent assay (G-LISA) to determine total Rac1 activity, we observed that the simultaneous inactivation of both Vav2 and Vav3 was required to reduce basal Rac1 activity in 4T1 cells (Fig. 1A). In contrast, the overexpression of a single Vav family protein, but not the catalytically inactive $Vav2^{R373A}$ mutant, restored normal Rac1 activity in the *Vav;Vav3* knockdown cell line (Fig. 1A). Similar results were found when Rac1 activity was determined by standard pull-down experiments with a glutathione *S*-transferase (GST) fusion protein containing the Rac1 binding domain of p21 protein (Cdc42/Rac)–activated protein kinase 1 (Pak1) (Fig. 1B). The elimination of Vav proteins in 4T1 cells did not affect basal RhoA activity (Fig. 1A).

When implanted in the mammary fat pads of recipient mice, all *Vav* knockdown cell lines developed tumors with slow growth kinetics (Fig. 1, C to F). The examination of tumor-bearing animals at the end of the tumorigenesis assays also indicated that the metastasis of cancer cells to the lung was impaired upon depletion of either Vav2 or Vav3 and was abolished upon the simultaneous elimination of both Vav proteins (Fig. 1, G to I, and table S4). This defect was tissue-specific because all Vav-deficient tumors metastasized well to lymph nodes and spleen (table S4). These defects were observed with two independent knockdown cell clones, indicating that they represent a bona fide representation of the biological properties of Vav proteins (Fig. 1, C, D, and G, and table S4). Ectopic coexpression of both Vav proteins in *Vav2;Vav3* knockdown cells rescued primary tumorigenesis (Fig. 1E) and lung metastasis (Fig. 1H and table S4) to the extent seen with the control cell line. By contrast, the reexpression of any of the two single Vav proteins (Fig. 1, E and H, and table S4) or the constitutively active $Vav2^{Y172F}$ mutant (Fig. 1F and table S4) failed to restore the tumorigenic properties of *Vav2;Vav3* knockdown cells. Because basal Rac1 activity in Vav2-, $Vav2^{Y172F}$-, Vav3-, and Vav2/Vav3-reconstituted *Vav2;Vav3* knockdown cells is not significantly different (Fig. 1, A and B), this result suggests that Vav2 and Vav3 act nonredundantly in tumorigenesis and lung metastasis, likely by engaging both Rac1-dependent and Rac1-independent routes. This idea is also consistent with the observation that the single-knockdown Vav2 and Vav3 4T1 cells show defects in both primary tumorigenesis (Fig. 1C) and metastasis (Fig. 1G) despite showing basal Rac1 activity comparable to that found in control cells (Fig. 1A).

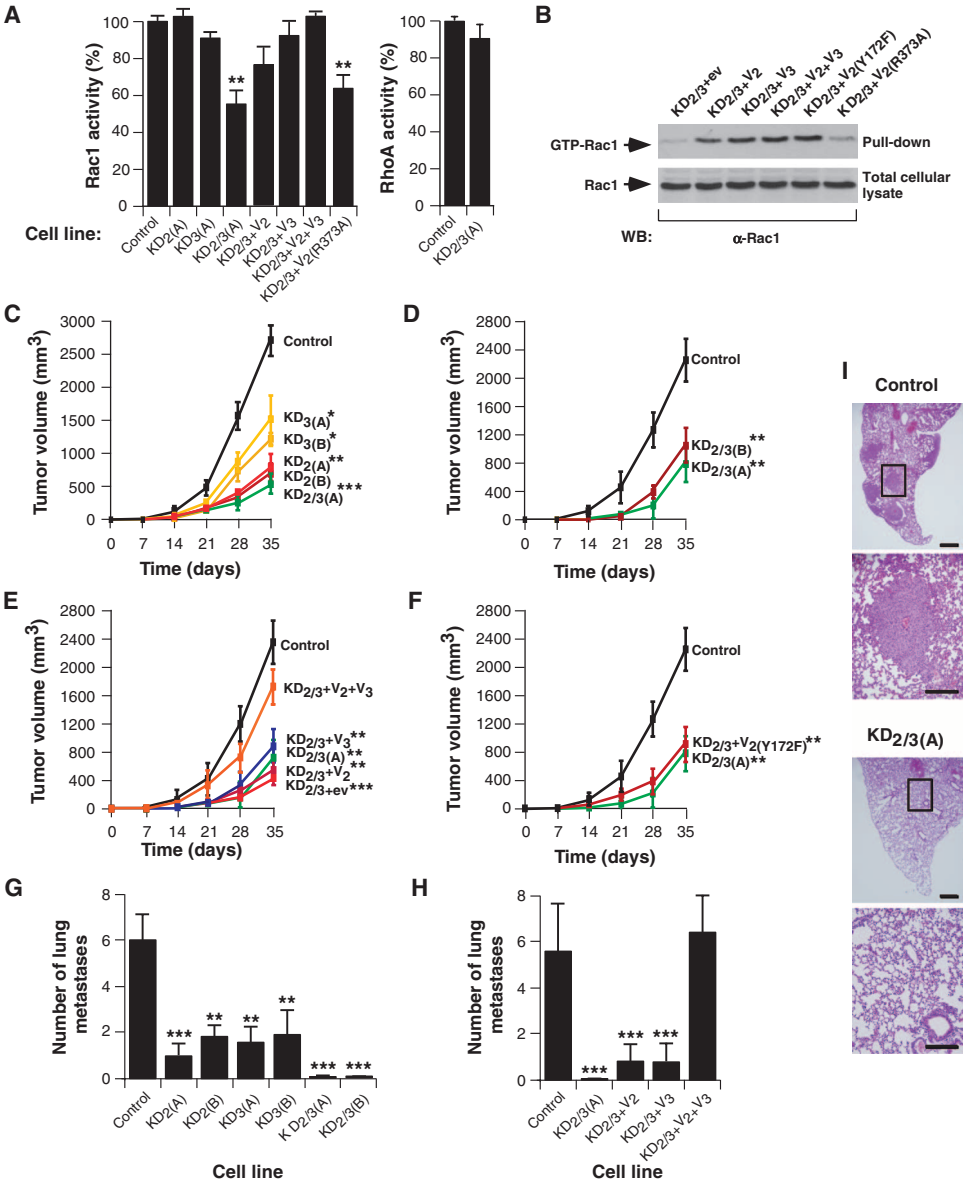

Fig. 1. Defective tumorigenesis and lung metastasis of Vav-deficient 4T1 cells. (**A** and **B**) Rac1 (A and B) and RhoA (A) activity was calculated in the indicated cell lines by G-LISA (A) and GST-Pak1 pull-down (B) experiments (n = 3 experiments). KD, knockdown cell line. Table S3 contains a description and designation of the cell lines used in these experiments. (**C** to **F**) Growth kinetics of tumors induced by the indicated cell lines. Statistics were performed at the 35-day time point. The number of independent samples in (C) was as follows: control, n = 15; $KD_{2(A)}$, n = 4; $KD_{2(B)}$, n = 4; $KD_{3(A)}$, n = 4; $KD_{3(B)}$, n = 4; $KD_{2/3(A)}$, n = 8. In (D) and (E), n = 8; in (F), n = 4. (**G** and **H**) Number of metastatic nodules detected in mice harboring tumors induced by the indicated cell lines (n = 5 animals). (**I**) Images showing the lack of macro- and micrometastasis in the lung of a mouse containing a tumor-derived $KD_{2/3(A)}$ cells. As control, we included a lung section from a mouse harboring a tumor derived from the control cell line. Scale bars, 100 μm (top image of each group) and 200 μm (bottom image of each group).

Vav proteins have pleiotropic functions in breast cancer

To further evaluate the effect and functional redundancy of Vav proteins on primary tumor growth, we studied the implication of each of those proteins in various cancer-linked processes. Using immunohistochemical techniques, we observed that the tumors derived from *Vav2;Vav3* knockdown cells showed reduced proliferation (as assessed by staining for Ki67) (Fig. 2, A and B) and neoangiogenesis (Fig. 2, C and D). The vessels generated inside those tumors were also less leaky than those found in control samples, as assessed by in vivo permeability experiments with intravenously injected rhodamine-labeled dextran (Fig. 2, E and F). Rescue of proliferation, neoangiogenesis, and leakiness required the simultaneous reintroduction of Vav2 and Vav3 in *Vav2;Vav3* knockdown cells (Fig. 2, A to F). The absence of both Vav proteins also increased the number of apoptotic, TUNEL (terminal deoxynucleotidyl transferase–mediated deoxyuridine triphosphate nick end labeling)–positive cancer cells, suggesting a role for those proteins in cancer cell survival (Fig. 2, G and H). However, this defect could be corrected by re-expressing either Vav protein in *Vav2;Vav3* knockdown cells (Fig. 2, G and H), indicating that Vav2 and Vav3 regulate this latter route redundantly.

We analyzed the effect of Vav2 and Vav3 on the intravasation, extravasation, and lung colonization properties of breast cancer cells. We quantified the number of circulating cancer cells in tumor-bearing animals and found that *Vav2;Vav3* knockdown cells intravasated threefold less efficiently than control cells (Fig. 3A). However, this defect could not explain the lack of lung metastasis exhibited by those tumors because the *Vav2;Vav3* knockdown cells could develop metastases in other secondary tissues (table S4). Consistent with this observation, we noticed that *Vav2;Vav3* knockdown cells could not metastasize to the lung even when introduced intravenously in recipient mice (Fig. 3, B to E), suggesting that Vav deficiency affects post-intravasation steps during metastasis. To investigate this possibility, we intravenously injected cancer cells that had been labeled with a cell-permeable chromophore and evaluated their extravasation to the lungs of recipient mice by confocal microscopy. These experiments indicated that *Vav2;Vav3* knockdown cells could not colonize the lung (Fig. 3, F and G). In fact, when detected, they were usually visualized as single cells trapped inside the lung capillaries (Fig. 3F). The simultaneous reintroduction of Vav2 and Vav3 was required to restore these intravasation (Fig. 3A) and post-intravasation steps during metastasis (Fig. 3, E to G) in *Vav2;Vav3* knockdown 4T1 cells.

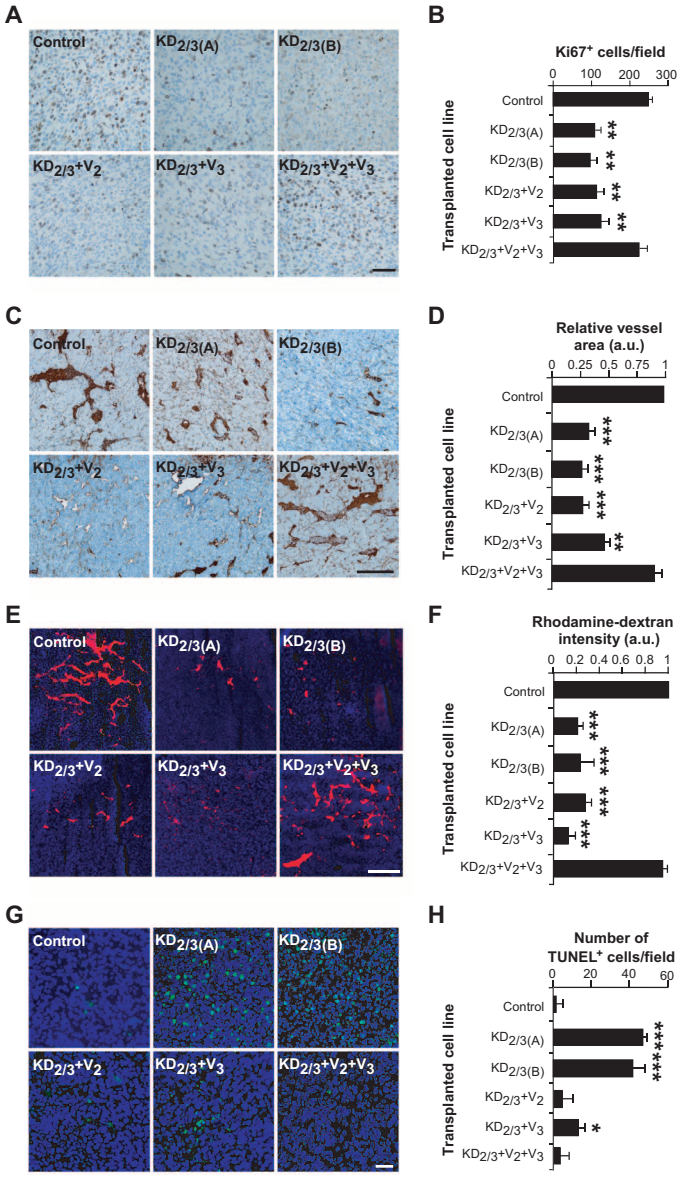

Fig. 2. Vav family proteins have overlapping, but not identical, roles in primary tumorigenesis. (**A** and **B**) Example (A; scale bar, 50 μm) and quantitation (B; $n = 3$ sections per tumor, four animals) of the proliferation of tumors derived from the indicated cell lines. (**C** and **D**) Example (C; scale bar, 100 μm) and quantitation (D; $n = 3$ sections per tumor, three animals) of angiogenesis in tumors developed from the indicated cell lines. (**E** and **F**) Examples (E; scale bar, 100 μm) and quantification (F; $n = 2$ sections per tumor, three animals) of the vessel permeability of tumors derived from the indicated cell lines. (**G** and **H**) Example (G; scale bar, 50 μm) and quantification (H; $n = 3$ sections per tumor, four animals) of apoptosis in tumors derived from the indicated cell lines.

Vav proteins play protumorigenic and prometastatic roles in both primary breast epithelial cells and nonmetastatic breast cancer cell lines

To ensure that the role of Vav proteins in breast cancer was not limited to 4T1 cells, we also used independent experimental systems. As a first approach, we investigated whether the absence of Vav2 and Vav3 affected the transformation of the mammary gland induced by polyomavirus middle T antigen (PyMT). We isolated primary breast epithelial cells from wild-type and *Vav2*$^{-/-}$;*Vav3*$^{-/-}$ mice and, after transducing them with a lentivirus containing the *PyMT* oncogene, reimplanted them in the mammary fat pads of female mice to follow the kinetics of mammary tumor formation in vivo. Unlike wild-type cells, the PyMT-transduced *Vav2*$^{-/-}$;*Vav3*$^{-/-}$ cells could not develop tumors or metastases when implanted in recipient mice (Fig. 4, A and B).

As a second approach, we investigated whether the overexpression of Vav2 and Vav3 could confer metastatic properties on 168FARN cells. Although isolated from the same mouse mammary carcinoma as 4T1 cells, 168FARN cells are not metastatic due to severe defects in both intravasation and post-intravasation steps (*24*). Although the overexpression of the two Vav proteins in 168FARN cells (Fig. 4C) did not lead to increased Rac1 activity in vitro (Fig. 4D), it promoted faster tumor growth kinetics (Fig. 4E) as well as lung metastasis (Fig. 4F) in vivo. These cells could also infiltrate efficiently the spleen (Fig. 4F), indicating that overexpression of Vav2 and Vav3 eliminates the defective intravasation step of 168FARN cells. Vav2- and Vav3-overexpressing 168FARN cells, but not the control counterparts, also formed lung metastasis when intravenously injected in mice (Fig. 4G). Together, these data indicate that Vav proteins promote breast cancer tumorigenesis as well as the intravasation and extravasation steps of metastatic breast cancer cells.

Vav2 and Vav3 regulate the transcriptome of breast cancer cells through common, synergistic, and isoform-specific pathways

To investigate whether the need for both Vav family proteins in breast tumorigenesis and metastasis reflected their contribution to the intrinsic proliferative and migratory properties of breast cancer cells, we evaluated these two parameters in our collection of 4T1 cells in vitro. *Vav2;Vav3* knockdown cells showed significantly lower proliferation (Fig. 4H) and invasion (Fig. 4I) rates than control cells. However, unlike the results obtained in orthotopically transplanted cells, the rescue of those two in vitro defects could be efficiently achieved by overexpressing Vav2 in *Vav2;Vav3* knockdown cells (Fig. 4, H and I). These results, together with the observations in Figs. 1 to 3, suggested that the synergistic functional interaction of Vav2 and Vav3 in breast cancer cells cannot be attributed unilaterally to their expected action on overall Rac1 activity, migration, or proliferation.

These results led us to carry out Affymetrix microarray experiments to identify distal effectors that could explain the cooperative action of Vav2 and Vav3 in breast cancer. We identified 2411 transcripts showing altered abundance upon depletion of both Vav proteins in 4T1 cells (fig. S3A and table S5). Using various both experimental and therapeutic-oriented criteria (such as mRNAs with reduced abundance in *Vav2;Vav3* knockdown cells that encoded therapeutically amenable proteins), we selected six transcripts showing reduced abundance in *Vav2;Vav3* knockdown 4T1 cells for further functional characterization (*Itgb6*, *Itga8*, *Ilk*, *Tacstd2*, *Inhba*, and *Ptgs2*). *Itgb6* and *Itga8* encode integrin subunits that regulate cell adhesion to laminins and fibronectin, respectively (*25*). *Ilk* encodes integrin-linked kinase, a pseudokinase that is an adaptor protein downstream of integrins (*26*). *Tacstd2* (tumor-associated calcium signal transducer 2) encodes an epithelial cell adhesion molecule (EpCAM) family member with roles in cell adhesion and cell signaling (*27*). *Inhba* encodes inhibin βA (InhβA), a ligand of the transforming growth factor–β family that can form homodimers or heterodimers with Inhα and InhβB subunits (*28*). *Ptgs2* encodes cyclooxygenase 2 (Cox2), an endoplasmic reticulum–localized enzyme involved in prostaglandin production (*29*). This latter protein was chosen as a positive control because it had been previously linked to metastatic processes (*30*).

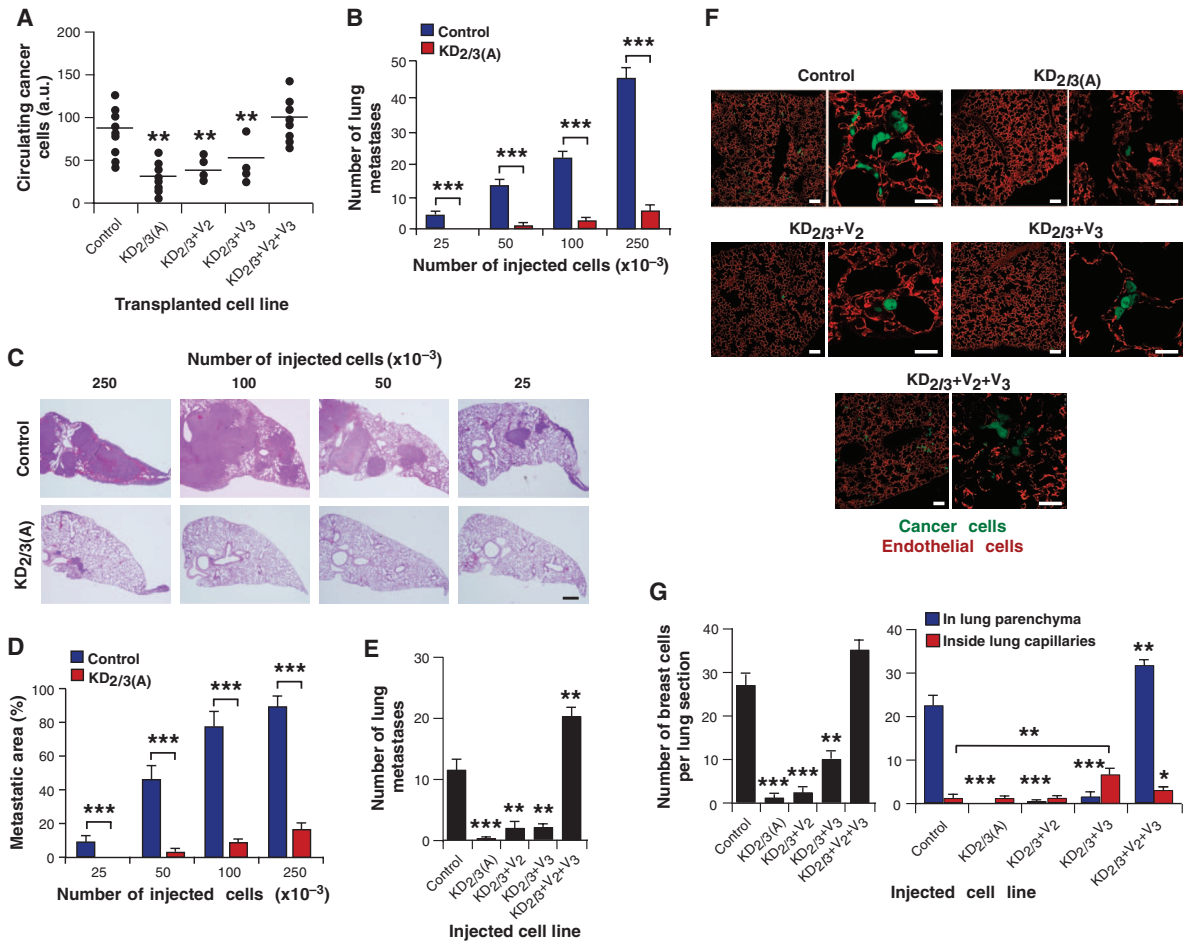

Fig. 3. Vav proteins function during several metastatic stages. (A) Percentage of circulating cancer cells in mice with tumors derived from the indicated cell lines [$n = 8$ in experiments with control, $KD_{2/3(A)}$, and $KD_{2/3} + V_2/V_3$ cells, and $n = 4$ for the rest of the experiments]. a.u., arbitrary units. (B to E) Number of metastases (B and E) and extent of metastasis (C and D) formed in the lung by the indicated intravenously injected cell lines ($n = 3$ lung sections per mice, four mice in each experimental condition). Scale bar, 100 μm. (F) Lungs from mice intravenously injected with the indicated chromophore-labeled cell lines were imaged by confocal microscopy to visualize cancer cells (green) and the vascular endothelium (red). Scale bars, 100 μm (left image of each group) and 25 μm (right image of each group). (G) Quantification of the number of chromophore-labeled cancer cells in either whole lung sections (left) or the indicated lung locations (right) ($n = 6$ confocal sections per animal, four mice in each condition).

We confirmed by qRT-PCR that the selected Vav-dependent transcripts were less abundant in cultured *Vav2;Vav3* knockdown cells (fig. S3B) and in the primary tumors derived from them (fig. S3C) than in parallel samples obtained from control cells. With the exception of the *Ptgs2* mRNA, these transcripts were also less abundant in the nonmetastatic 168FARN than in the metastatic 4T1 cells (fig. S3D). The overexpression of Vav2 and Vav3 in 168FARN cells, which conferred metastatic properties (Fig. 4, F and G), increased the abundance of most of those transcripts to values either similar to (*Itga8* and *Ilk*) or higher than (*Inhba* and *Ptgs2*) those found in 4T1 cells (fig. S3D). The exceptions were *Itgb6*, which did not show increased abundance, and *Tacstd2*, which showed only a twofold increase in abundance (fig. S3D). Given the cooperative effect of Vav2 and Vav3 in tumor growth and metastasis, we next investigated the abundance of the selected Vav family targets in single Vav2–, single Vav3–, and double Vav2/Vav3–reconstituted *Vav2;Vav3* knockdown cells (fig. S4A). Reintroducing either Vav protein in *Vav2;Vav3* knockdown cells returned the abundance of *Itga8*, *Tacstd2*, and *Ptgs2* mRNAs to control or higher-than-control amounts. By contrast, the rescue of *Ilk* and *Inhba* transcript abundance to control or higher-than-control amounts required the simultaneous reintroduction of both Vav proteins. *Itgb6* transcript abundance was restored to control amounts by overexpressing Vav3, but not Vav2, in *Vav2;Vav3* knockdown cells (fig. S4A).

To determine whether Rac1 was involved in regulating the Vav2/Vav3-dependent transcriptome, we stably expressed a constitutively active, fast-cycling Rac1 mutant (F28L) in both control and *Vav2;Vav3* knockdown cells (fig. S4, B and C). G-LISA experiments indicated that the presence of $Rac1^{F28L}$ bypassed the deficient activation of endogenous Rac1 induced by the compound *Vav2;Vav3* knockdown in 4T1 cells (fig. S4D). In fact, Rac1 activity was higher in $Rac1^{F28L}$-expressing cells than in normal 4T1 cells independently of the abundance of endogenous Vav proteins (fig. S4D). When expressed in *Vav2;Vav3* knockdown cells, $Rac1^{F28L}$ could not rescue the abundance of the *Ilk* transcript, thus confirming the idea that some of the downstream effects of Vav proteins were Rac1-independent (fig. S4E). In fact, when expressed in normal 4T1 cells, $Rac1^{F28L}$ reduced

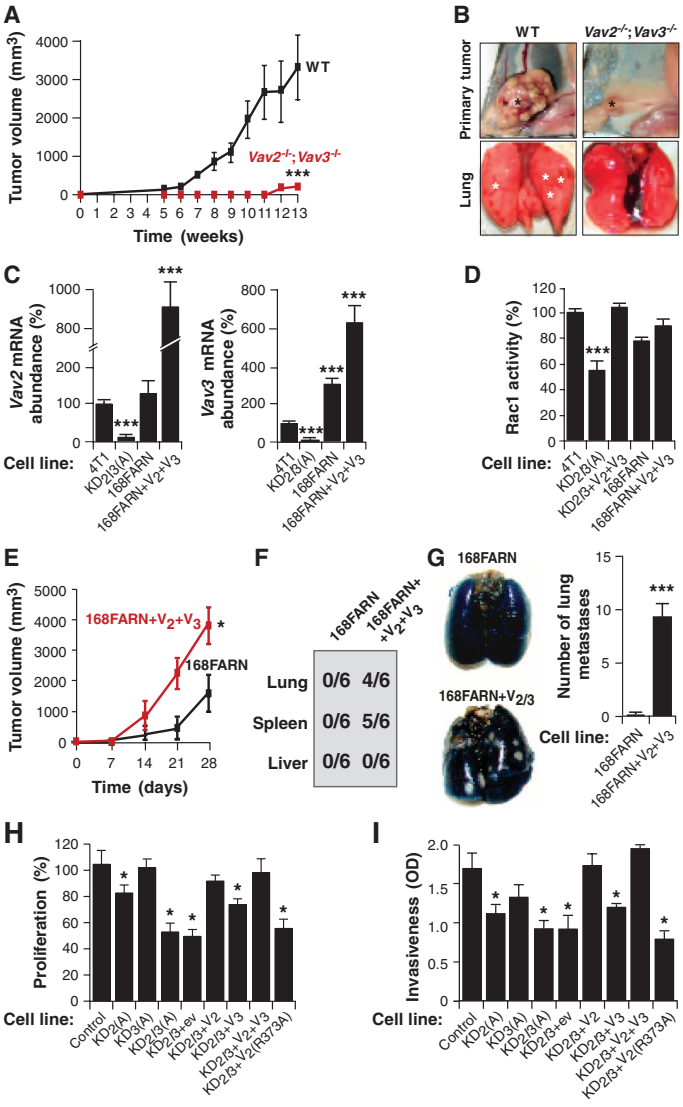

Fig. 4. Protumorigenic and prometastatic roles of Vav proteins in independent experimental systems. (**A** and **B**) Primary tumorigenesis (A and B) and lung metastasis (B) induced by *PyMT*-transformed wild-type (WT) and *Vav2*$^{-/-}$;*Vav3*$^{-/-}$ primary breast epithelial cells upon implantation in the fat pads of recipient WT female mice (n = 11 animals per genotype). (**C**) Abundance of *Vav2* (left) and *Vav3* mRNAs (right) in the indicated cells (n = 3 experiments). (**D**) Rac1 activity in the indicated cell lines detected with G-LISA assays (n = 3 experiments). (**E** and **F**) Growth kinetics of breast tumors formed by the indicated orthotopically transplanted cell lines (E) (n = 6 animals). In (F), the x/y ratio indicates the number (x) of animals that scored positive for metastasis in the indicated tissues compared to the total number (y) of mice analyzed in these experiments. (**G**) Example (left) and quantification (right) of metastases generated by the indicated intravenously injected cell lines (n = 4 animals). (**H** and **I**) In vitro proliferative (H) and invasion (I) properties of the indicated cell lines (n = 3 experiments). OD, optical density.

the abundance of the *Ilk* mRNA (fig. S4E). By contrast, the Rac1 mutant restored the abundance of the other synergistic target (*Inhba*) and the two mRNAs that were commonly regulated by Vav2 and Vav3 (*Tacstd2* and *Ptgs2*) to control or higher-than-control amounts in *Vav2;Vav3* knockdown cells (fig. S4E). The increase in the abundance of both the *Inhba* and *Ptgs2* mRNAs that was induced by Rac1^{F28L} expression was significantly higher in wild-type 4T1 cells than in *Vav2;Vav3* knockdown cells (fig. S4E). Because the abundance (fig. S4, B and C) and activity (fig. S4D) of Rac1^{F28L} in these two cell lines were similar, this result suggests that Rac1-independent pathways triggered by either Vav2 or Vav3 may be required for the optimal regulation of these distal downstream targets.

To further verify the implication of GEF-independent routes in the engagement of the distal Vav family–dependent transcriptomal program, we investigated whether the synergistic response previously observed between Vav2 and Vav3 in the regulation of *Ilk* and *Inhba* mRNA abundance (fig. S4A) could be reproduced in *Vav2;Vav3* knockdown cells reconstituted with wild-type Vav3 and catalytically inactive Vav2^{R373}. The abundance of the transcripts for these two ectopic proteins in the reconstituted knockdown cell line is shown in fig. S4F. These experiments demonstrated that the contribution of Vav2 to the regulation of *Ilk* gene expression was independent of its enzymatic activity (fig. S4G). By contrast, Vav2 required GEF activity to synergize with wild-type Vav3 in regulating the abundance of *Inhba* mRNA (fig. S4G). The latter result suggests that the synergism observed between Vav proteins in the regulation of this gene is probably due to the stimulation of different spectra of Rho GTPases by Vav2 and Vav3 or, alternatively, by the Vav family member–specific activation of Rac1 in different subcellular localizations. The restoration of all Vav family GEF–dependent and GEF-independent pathways seems to be crucial for the efficient metastasis of cancer cells to the lung because Rac1^{F28L}- and Vav3/Vav2^{R373A}-expressing *Vav2;Vav3* knockdown cells did not efficiently metastasize to the lung when injected intravenously in mice (fig. S4H). Together, these results indicate that (i) Vav proteins control gene expression through common, synergistic, and Vav family member–specific pathways; (ii) the targets commonly regulated by Vav2 and Vav3 use exclusively Rac1-dependent (*Tacstd2*) or Rac1-dependent plus Rac1-independent (*Ptgs2*) pathways; and (iii) the synergistic targets can be regulated through either GTPase-independent (*Ilk*) or GTPase-dependent (*Inhba*) routes (fig. S4I).

To estimate on a genome-wide level the number of Vav family "common" (mRNAs whose abundance is indistinctly regulated by any of the two Vav proteins), "synergistic" (mRNAs whose abundance requires simultaneous signaling inputs from Vav2 and Vav3), and "isoform-specific" (transcripts whose abundance is regulated exclusively by one Vav family member) transcriptomal subsets, we compared the transcriptome of *Vav2;Vav3* knockdown cells and Vav2-, Vav3-, and Vav2/Vav3-reconstituted *Vav2;Vav3* knockdown cells by microarray analyses. The bioinformatics analysis of the data obtained revealed that 36.4, 23.5, and 35.5% of the Vav family–dependent transcriptome could be assigned to the common-, synergistic-, and Vav3-dependent subclasses, respectively (fig. S5). By contrast, the percentage of Vav2-specific genes was significantly lower in the overall Vav family–dependent transcriptome (4.6%; fig. S5).

Vav-dependent targets have overlapping, but not identical, roles in breast cancer

We next knocked down each of the six selected Vav target genes in 4T1 cells to address their roles in breast cancer (fig. S6 and table S3). Similar to Vav proteins, we found that Ilk, Tacstd2, InhβA, and Cox2 were important for optimal tumor growth (Fig. 5A) and lung-specific metastasis (Fig. 5B). These data were obtained with two knockdown cell clones generated with two independent short hairpin RNAs (shRNAs) for each target (Fig. 5, A and B), thus ruling out the possibility of spurious, off-target effects. The analysis of tumors derived from these knockdown cell lines indicated that Ilk, Tacstd2, InhβA, and Cox2 were critical for cancer cell proliferation (Fig. 5, C and D) and intratumoral angiogenesis (Fig. 5, E and F). By contrast, InhβA and Ilk

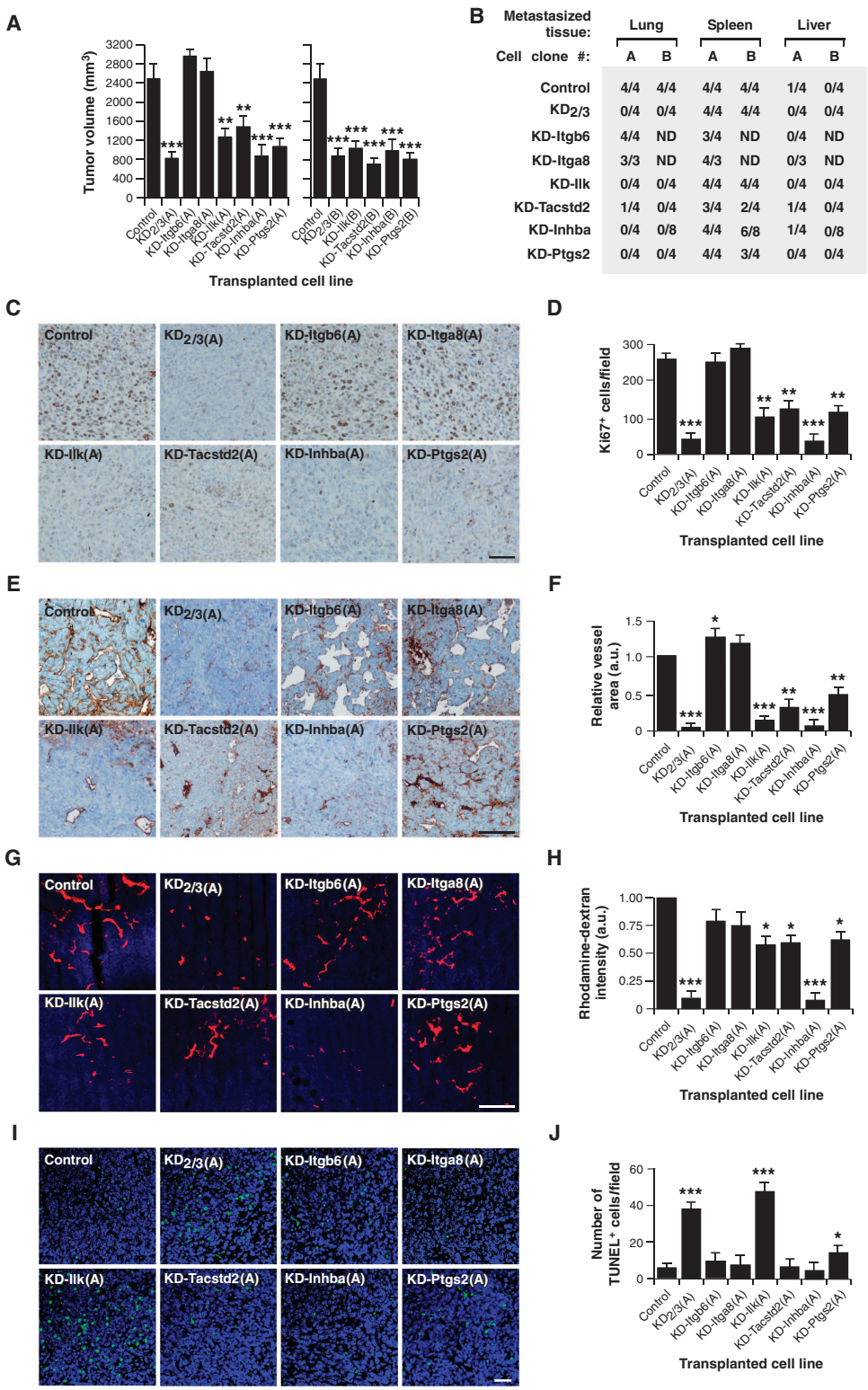

Fig. 5. Vav family targets play overlapping, but not identical, roles in biological processes linked to primary tumorigenesis. (**A**) Growth of tumors derived from the indicated orthotopically transplanted cell lines (n = 4 animals). KD, knockdown cell. Clones A and B refer to two knockdown cell clones generated with two independent shRNAs for the indicated target (see also table S3). (**B**) Metastases found in tissues (top) of mice bearing tumors from the indicated cell clones. Values are given as in Fig. 4F. ND, not determined. (**C** and **D**) Example (C; scale bar, 50 μm) and quantitation (D; n = 3 sections per tumor, four animals) of the proliferation of tumors derived from the indicated cell lines. (**E** and **F**) Example (E; scale bar, 100 μm) and quantitation (F; n = 3 sections per tumor, three animals) of angiogenesis in tumors derived from the indicated cell lines. (**G** and **H**) Example (G; scale bar, 100 μm) and quantitation (H; n = 2 sections per tumor, three animals) of the vessel permeability of tumors derived from the indicated cell lines. (**I** and **J**) Example (I; scale bar, 50 μm) and quantitation (J; n = 3 sections per tumor, three animals) of apoptosis in tumors from the indicated cell lines.

had critical roles in vascular permeability and cancer cell survival, respectively (Fig. 5, G to J). The elimination of Itgβ6 or Itgα8 did not show any deleterious effect on any of those biological parameters (Fig. 5).

Measuring the number of circulating cancer cells in tumor-bearing animals revealed that InhβA was the only target that promoted cancer cell intravasation (Fig. 6A). By contrast, the extravasation step depended on Ilk, Tacstd2, and, to a lower extent, InhβA (Fig. 6, B and C). Consistent with these data, long-term metastasis experiments with intravenously injected cancer cells indicated that both Ilk and Tacstd2 were critical for the formation of metastatic nodules in the lung (Fig. 6, D to F). These experiments also revealed that InhβA and Cox2 were key for the formation of metastatic nodules in that tissue (Fig. 6, D to F). Because those two proteins are not important for extravasation (Fig. 6, B and C), this result suggests that they play roles in the fitness of cancer cells once they reach the lung parenchyma. *Itgb6* and *Itgα8* knockdown cells did not show defects in any of the these metastatic stages (Fig. 6).

The role of InhβA and Cox2 in post-extravasation stages led us to investigate whether Vav proteins and the other Vav targets could also regulate the fitness of cancer cells inside the lung parenchyma. Because the extravasation defect of *Vav2;Vav3*, *Ilk*, and *Tacstd2* knockdown cells precluded the direct examination of that issue, we artificially facilitated their extravasation in vivo by treating the mice with monocrotaline, a toxin that

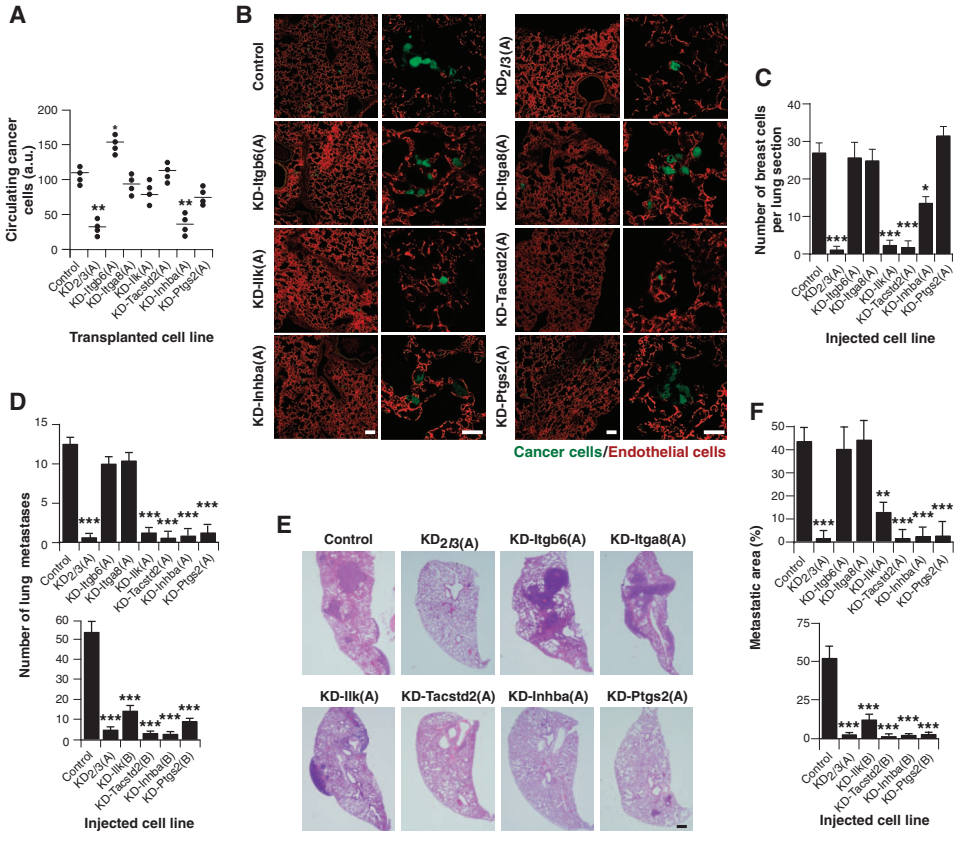

Fig. 6. Role of Vav-dependent targets in the metastatic steps of breast cancer cells. (**A**) Percentage of circulating cancer cells present in mice harboring tumors derived from the indicated cell lines (n = 4 animals). The description of each cell line can be found in table S3. (**B** and **C**) Visualization (B) and quantification of the extravasation rates (C) of the indicated chromophore-labeled cell lines after intravenous injection into mice. Scale bars in (B), 100 μm (left image of each group) and 25 μm (right image of each group) (n = 6 confocal sections per animal, four mice in each condition). (**D** to **F**) Number (D) and extent (E and F) of the metastatic nodules formed by the indicated intravenously injected cell lines (n = 3 independent lung sections per mice, four mice in each condition). Scale bar, 100 μm.

increases the permeability of the lung vascular endothelium (*31*). We speculated that such an approach could facilitate the movement of the knockdown cells across the endothelial layer. Consistent with this hypothesis, we observed that monocrotaline favored the efficient extravasation of all the knockdown 4T1 cells tested, although it did not improve the already high extravasation rates of control cells (Fig. 7, A and B). Nevertheless, *Vav2;Vav3*- and *Tacstd2*-deficient cells could not form lung metastases in monocrotaline-treated mice, indicating that, similarly to the previously characterized InhβA and Cox2 proteins (see above, Fig. 6, D to F), those proteins participated in the intraparenchymal fitness of cancer cells (Fig. 7, C to E). By contrast, *Ilk* knockdown cells formed metastatic nodules in a monocrotaline-dependent manner (Fig. 7, C to E), demonstrating that the function of Ilk is limited to the extravasation step. Together, these results indicate that Vav2 and Vav3 regulate many of the steps involved in the colonization of the lung by metastatic breast cancer cells by controlling the abundance of prometastatic distal targets through both common and synergistic routes (Fig. 7F).

The Vav2/Vav3-dependent transcriptome harbors prognostic gene signatures for breast cancer

To investigate the potential clinical interest of the Vav pathway in breast cancer, we determined the prognostic value of the Vav2/Vav3-dependent transcriptome. The initial use of a small gene signature composed of *Vav2*, *Vav3*, *Ilk*, *Inhba*, *Tacstd2*, and *Ptgs2* in human breast cancer data sets was not informative in terms of disease outcome prediction. Because the dual role of their encoded products in primary tumorigenesis and metastasis could interfere with patient stratification into different prognostic categories, we decided to interrogate the entire Vav2/Vav3-dependent transcriptome to obtain clinically informative gene signatures. To this end, we used all the Vav-dependent transcripts that, according to the microarray experiments shown in figs. S4A and S5, displayed consistent changes in abundance between the metastatic (control and Vav2/Vav3-reconstituted *Vav2;Vav3* knockdown cells) and the nonmetastatic cell lines (*Vav2;Vav3* knockdown cells). This strategy allowed us to eliminate transcripts whose abundance was not rescued by the reintroduction of Vav2 and Vav3 in the *Vav2;Vav3* knockdown cell lines. In addition, it eliminated transcripts whose abundance was modified only during Vav overexpression. This approach led to the identification of 1546 Vav2/Vav3-dependent mRNAs whose abundance correlated with the metastatic potential of our cell lines (fig. S7A and table S6). After mapping the mRNAs to their human counterparts, we investigated whether their abundance was associated with disease outcome using human breast tumor mRNA microarray data sets. We found that patients with significant overlaps with the Vav2/Vav3-dependent mRNA signature had worse prognosis in terms of overall survival (table S7), tumor recurrence (table S7), or metastatic events (fig. S7, B and C, and table S7). To further confirm that Vav2/Vav3-regulated genes served as lung metastatic predictors, we next generated a minimal Vav2/Vav3 prognostic lung metastatic signature (V2/V3LMS). By training our 1546 mRNA signature with the Wang breast cancer data set (*32*), we established a classifier group of 102 mRNAs capable of predicting lung metastasis in breast cancer (table S8). We observed that, when used to stratify patients, the V2/V3LMS could predict lung metastasis–free survival in breast cancer patients in both the NKI (Netherlands Kancer Instituut) (fig. S7D) and MSKCC (Memorial Sloan-Kettering Cancer Center) (fig. S7E) cohorts (*33*, *34*). By contrast, and in agreement with our biological data, it did not have any prognostic value for bone metastasis–free survival (fig. S7F). The V2/V3LMS behaves similarly or better than previously reported gene signatures with diagnostic value to forecast lung metastasis development in human patients (*33*, *34*) (fig. S7G).

DISCUSSION

Here, we have demonstrated that Vav2 and Vav3 regulate biological parameters critical for the growth of breast tumors and their metastatic dissemination to the lung (Fig. 7F). The effect of those proteins in primary tumorigenesis is not fully penetrant because the depletion of both GEFs

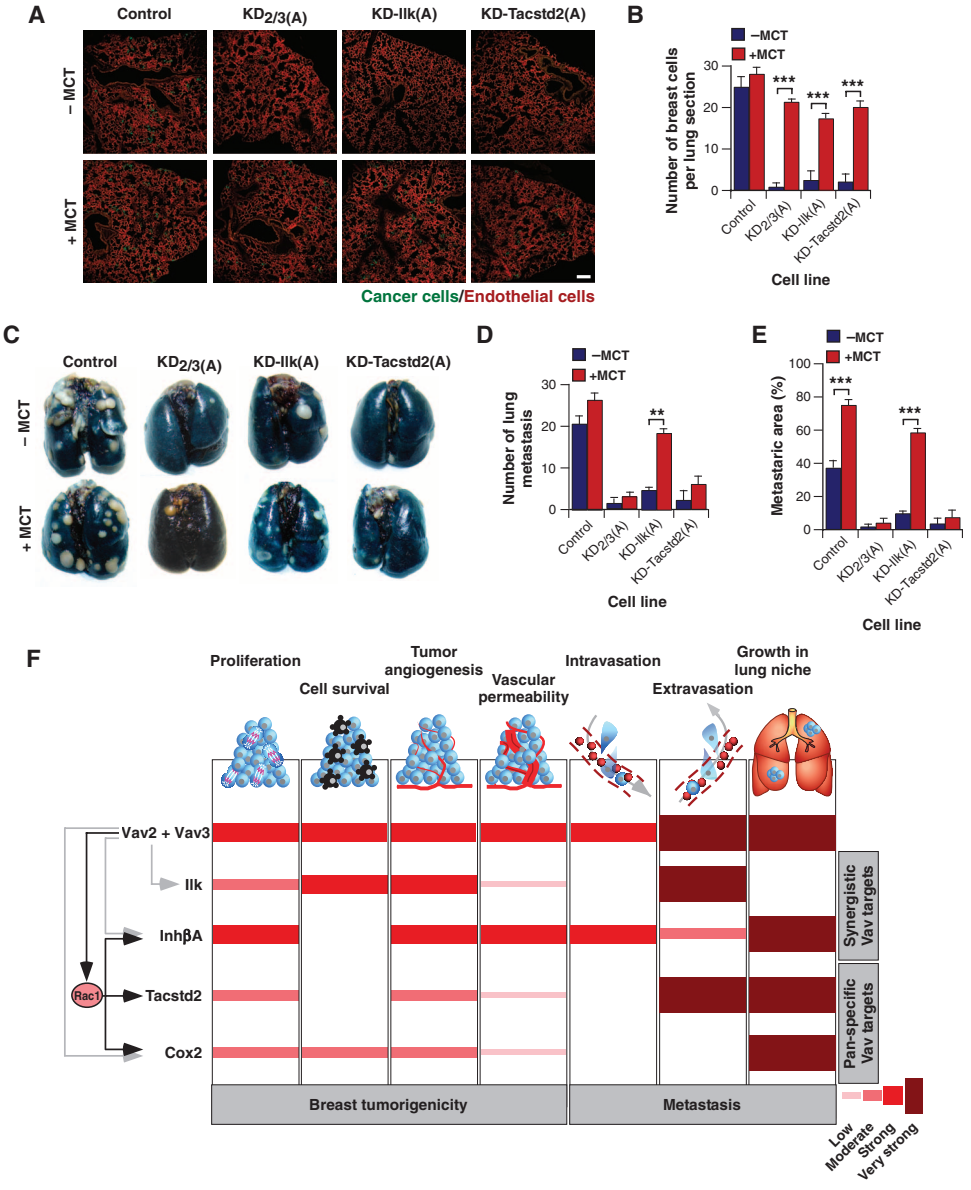

Fig. 7. The Vav pathway is involved in the survival of cancer cells inside the lung. (**A** and **B**) Visualization (A; green color; scale bar, 100 μm) and quantification (B; $n = 6$ confocal sections per animal, four mice in each condition) of the extravasation of the indicated chromophore-labeled cell lines after intravenous injection in monocrotaline-treated (+MCT) and untreated (–MCT) mice. Endothelial cells are labeled in red in (A). (**C** and **D**) Visualization (C) and quantification (D; $n = 4$ mice) of the metastatic nodules induced by the indicated cell lines after intravenous injection in MCT-treated (+MCT) or untreated (–MCT) mice. (**E**) Area of the metastatic nodules generated by the indicated cell lines in the lung parenchyma ($n = 3$ sections per mice, four mice per experimental condition). (**F**) Summary of our results. The importance of a protein in the indicated process is proportional to the thickness and darkness of horizontal bars. Rac1-dependent and Rac1-independent routes are depicted in black and gray arrows, respectively. We cannot rule out the possibility that Ilk abundance is regulated by Vav3-mediated stimulation of another Rho GTPase. However, Vav2 contributes to this response in a GEF-independent manner.

delays, but does not abate, breast tumor growth in the 4T1 model. By contrast, they are essential for lung metastasis, as assessed by the absence of metastatic nodules or micrometastases in animals orthotopically transplanted with *Vav2;Vav3*-deficient breast cancer cells. Indeed, lung metastasis cannot develop even under very permissive experimental conditions such as the intravenous injection of large numbers of cancer cells in recipient mice. This is a tissue-specific function because Vav-deficient cells do metastasize to other peripheral tissues. Such selectivity can be explained by the direct role of Vav proteins in the extravasation of breast cancer cells through the lung vascular endothelium, a tight physical barrier not found in the highly fenestrated vessels of bone or liver (*35*). In addition, they also contribute to the fitness of breast cancer cells inside the lung parenchyma, a niche that poses biological challenges for the ectopic proliferation and survival of cancer cells (*35*). The former function is perhaps the most relevant in this pathological context because *Vav2;Vav3*-deficient breast cancer cells extravasate only when the permeability of the endothelial barrier is artificially induced by pharmacological means (such as monocrotaline injections). We have also identified a role of Vav proteins in the intravasation step of metastatic breast cancer cells. Although this function is obviously not essential in our experimental setting, it may play more important roles in breast tumors with sizes more similar to those found usually in the clinic. Favoring this idea, we found that the overexpression of Vav2 and Vav3 eliminates the defective intravasation properties of the nonmetastatic 168FARN cancer breast cell line.

Our study has also revealed that Vav proteins control a large subset of the cancer cell transcriptome, including mRNAs encoding proteins that play critical roles in both primary tumorigenesis and lung-specific metastasis (Fig. 7F). This biological program is unique because it does not substantially overlap with previously described gene signatures associated with lung metastasis (*33*, *34*). Vav2 and Vav3 control these cancer-related processes using a combination of common and synergistic routes that, in turn, rely on both Rac1-dependent and Rac1-independent signals for full engagement (Fig. 7C). The analysis of the regulation of these transcripts shows an unexpected complexity. Thus, regulation of the abundance of some of the common (*Ptgs2*) and synergistic (*Inhba*) transcripts seems to rely on both Rac1-dependent and Rac1-independent signals (Fig. 7C). Congruous with this view, we found that constitutively active $Rac1^{F28L}$ increased the abundance of these two transcripts in a manner dependent on the abundance of Vav2 and Vav3 in breast cancer cells. Likewise, these two transcripts become more

abundant in 168FARN cells upon the overexpression of Vav2 and Vav3 under conditions that do not induce detectable variations in overall Rac1 activity. By contrast, the abundance of other targets commonly regulated by the two Vav proteins (*Tacstd2*) seems to rely exclusively on Rac1 signals in 4T1 cells (Fig. 7C). Finally, the abundance of other transcripts that rely on synergistic signals from the two Vav proteins (*Ilk*) is controlled by Vav2 in a catalytic and GTPase-independent manner (Fig. 7C). To add an additional layer of complexity to this regulatory mechanism, we observed that the rescue in the abundance of the synergistic *Inhba* transcript in *Vav2;Vav3* knockdown cells requires, in addition to wild-type Vav3–derived signals, signaling contributions from the catalytic domain of Vav2. Because overexpression of Vav3 is sufficient to rescue Rac1 activity in those cells, these results suggest that Vav3 and Vav2 may favor the specific activation of Rac1 in different subcellular localizations or, alternatively, that Vav2 may engage additional subsets of Rho proteins through its catalytic domain. These observations are consistent with other observations indicating that the knockdown of Vav2, but not Vav3, affects the proliferation and invasion of 4T1 cells in a GEF-dependent manner, although the overall Rac1 activity does not differ between control, single *Vav2* knockdown, single *Vav3* knockdown, and $Vav2^{R373A}$-reconstituted *Vav2;Vav3* knockdown cells. Although the targets identified in this work belong to the common and synergistic transcriptomal subclasses, it is possible that proteins whose abundance is modulated by either Vav2 or Vav3 through catalytic-dependent or catalytic-independent routes could also participate in this process. Further study of additional targets in the large Vav2/Vav3-dependent transcriptomal signature of breast cancer cells will be required to address this possibility.

Consistent with the role of the Vav family in breast cancer cell biology, our metagenomic analysis revealed that the abundance of the *Vav3* mRNA increases in samples from both specific breast cancer subtypes and immortalized breast cancer cell lines. Although the reason for the specific enrichment of the abundance of this Vav family transcript remains to be addressed experimentally, we speculate that it can be due to two different reasons. First, our microarray analyses have shown that Vav3 contributes to a larger extent than Vav2 to the regulation of the breast cancer Vav family–dependent transcriptome. This may indicate that, in addition to enhancing the regulation of common and synergistic targets, the overexpression of Vav3 could lead to a larger effect on the breast cancer cell transcriptome than Vav2. Second, the increase in abundance of human *Vav3* mRNA in breast cancer cells could merely reflect the specific inducible nature of its gene promoter. Consistent with this idea, we have reported previously that the expression of the *Vav3* gene, but not that of other *Vav* family genes, depends on the abundance of the transcription factor Ahr (aryl hydrocarbon receptor) in both mouse tissues and primary cells (*36*, *37*). Consistent with this, $Vav3^{-/-}$ and $Ahr^{-/-}$ mice display similar nervous system and cardiovascular defects (*37*). Additional experiments will be required to address this issue.

The present observations have also indirectly hinted at the mechanistic details of some of the metastatic steps of breast cancer cells. Thus, we have observed that the biological parameter of the primary tumor that correlates best with intravasation efficiency is the permeability of the intratumoral blood vessels. Consistent with this view, we found that the two knockdown cell lines that show lower vascular leakiness (*Vav2;Vav3*- and *Inhba*-deficient 4T1 cells) also show the most severe problems in intravasation (Fig. 7F). In addition, unlike other unrelated prometastatic biological programs (*30*), we have seen that the intravasation and extravasation steps do not require the same exact subsets of Vav-dependent target genes (Fig. 7F). This result suggests that the extravasation step is more functionally stringent than the intravasation step, probably because metastatic cells in the lung have to pass through an endothelium that, unlike the one present in the vasculature of the primary tumor mass, has not been "educated" by cancer cells to modify its normal histological structure and physiology. Alternatively, this functional specificity may be related to the stronger adhesion forces required to attach to the lung endothelium, given that this adhesion step is counterbalanced by shear forces induced by the blood flow inside the lung arterioles. Finally, we could not correlate the defects found in the primary tumor to the long-term fitness of the metastatic cells in the lung parenchyma (Fig. 7F). This suggests that, despite the fact that both processes require the engagement of common biological processes such as angiogenesis and proliferation (*38*, *39*), they are still controlled by different signaling mechanisms.

The circumscribed effect of Vav proteins on lung metastasis limits the potential interest of these GEFs and its distal downstream targets as general antimetastatic drug targets because it is clear that their inhibition will not limit the dissemination and growth of cancer cells in other peripheral tissues. Nevertheless, the observation that the elimination of Vav proteins, InhβA, Tacstd2, and Cox2 compromises the fitness of cancer cells in the lung parenchyma indicates that their inhibition could have some interest in the case of patients with metastasis circumscribed to the lung. In any case, the most obvious application of the present work is the observation that the Vav-dependent transcriptome harbors mRNA subsignatures capable of forecasting both disease outcome and lung metastasis in breast cancer patients. Prediction of this latter parameter is of obvious clinical interest because the lung is one of the main landing sites for metastatic breast cancer cells. In addition, it has a direct correlation with tumor recurrence and overall patient survival (*40*). The Vav-dependent gene signature identified here has no prognostic value for bone metastasis, a result that further underscores the tight functional link between the Vav route and the tropism of breast cancer cells to the lung.

The specific effect of Vav proteins on the late stages of lung metastasis raises additional questions regarding the participation of Rho GEFs in breast cancer tumorigenesis. For example, it will be interesting to determine whether the tumorigenic and metastatic steps that are less Vav2; Vav3-dependent are because other Rho GEFs control them. This is possible in the case of primary tumorigenesis because P-Rex1, a phosphatidylinositol 3-kinase–dependent Rac1 GEF (*2*, *3*) that shows high abundance in breast cancer [(*8*) and this work; fig. S1, A to E], is important for the growth of breast cancer cell lines in the primary tumor site (*8*). Thus, it is possible that P-Rex1, Vav2, and Vav3 could work in a combined fashion in that specific functional niche. At this point, however, there is no information about the role of P-Rex1 or other Rho GEFs in all the metastatic stages of breast cancer cells in vivo. It will be interesting therefore to functionally screen all the Rho GEFs that are either enriched or found at basal amounts in breast cancer (fig. S1, A and B) to dissect the specific contribution of each of them to the biological parameters tested in the present work. This would reveal the Rho GEF–dependent stages of the metastatic process and, in addition, the specific functional tasks that breast cancer–expressed GEFs play in that tumor. Finally, another question that remains to be addressed is whether the roles of Vav2 and Vav3 unveiled in this work are specific just for breast cancer cells or, alternatively, whether they are common to other metastatic tumors with tropism to ward the lung. Future work will be needed to tackle these lingering questions.

MATERIALS AND METHODS

Metagenomic analysis

The 54 Rho GEF family members were used together to interrogate the Oncomine/Compendia Bioscience database (https://www.oncomine.org/resource/login.html) (*41*) to identify those showing statistically significant

enriched abundance in specific types of human tumors, cancer cell lines, or healthy tissues. Score criteria for significant enrichment were as follows: analysis type, differential analysis; $P \leq 1 \times 10^{-4}$; fold change ≥2; gene rank, top 1%; number of tumor samples in microarray analysis, ≥151. Visualization of mRNA profiles was done with the tools present in the Oncomine/Compendia Bioscience. In all cases, the top 20 transcripts were graphically shown regardless of the statistical significance of their variation among samples. In the case of breast cancer subtypes (table S1), the screening criteria were the same as above, including the cancer type (breast cancer) as additional parameter. The analysis of the abundance of *Vav2* and *Vav3* mRNAs in luminal breast tumors (table S2) was done with a microarray breast cancer data set containing 508 samples (*42*). Intrinsic subtype classification and normalized microarray data were downloaded from the Gene Expression Omnibus (GEO) Web site (GSE25066). *Z* values were calculated from $\log_2$-based microarray abundance data for both mRNAs and the means and SEs calculated with analysis of variance (ANOVA).

Plasmid construction

To generate the lentiviral vector encoding hemagglutinin (HA)–tagged Vav2 (pCCM33), a complementary DNA (cDNA) fragment encoding mouse wild-type Vav2 was amplified by PCR with the pCMV-Vav2 plasmid as template (*43*). Primers were modified to introduce an Spe I site (underlined)/HA epitope (boldfaced) at the 5′ end and a Not I site (underlined) at the 3′ end in the amplified product. The sequences of the forward and reverse primers were 5′-AATAACTAGTGCCACCATG**TACCCATACGACGTCCCAGACTACGCT**GAGCAGTGGCGGCAATGCGGC-3′ and 5′-ATAGACCGCGGCCGCTCACTGGATGCCCTCCTCTTCTACGTA-3′, respectively. The amplified PCR cDNA fragment was digested with the indicated enzymes and cloned into a Spe I/Not I–linearized lentiviral vector (pLVX-IRES-Hyg, Clontech). The pCCM33 vector was subsequently used to generate plasmids encoding catalytically inactive (R373A mutant, pCCM36 vector) and catalytically active (Y172F mutant, pCCM35 vector) versions of HA-tagged Vav2 by site-directed mutagenesis (QuikChange Kit, Stratagene). Primers used to introduce those mutations were, for pCCM36, 5′-GTACATCAATGAAGTGAAGGCGGACAAGGAGACCTTGAAG-3′ (forward) and 5′-CTTCAAGGTCTCCTTGTCCGCCTTCACTTCATTGATGTAC-3′ (reverse), and for pCCM35, 5′-GATGAAGGAGATGACATTTTTGAGGACATCATCAGGGTG-3′ (forward) and 5′-CACCCTGATGATGTCCTCAAAAATGTCATCTCCTTCATC-3′ (reverse). To generate the lentiviral vector encoding Myc-tagged Vav3 (pCCM31), we amplified a cDNA fragment encoding mouse wild-type Vav3 by PCR with the pC.HA-Vav3 plasmid (Addgene) as template. Primers used in the amplification step were modified to introduce a Xho I site (underlined) and a Myc-tag (boldfaced) at the 5′ end, as well as a Not I site (underlined) at the 3′ end of the final cDNA product. The sequences of the forward and reverse primers were 5′-ATACTCGAGGCCACCATG**GAACAAAAACTTATTTCTGAAGAAGATCTG**GAGCCGTGGAAGCAGTGCGCT-3′ and 5′-ATAGACCGCGGCCGCTTATTCATCCTCTTCCACATATGTGG-3′, respectively. Upon digestion with Xho I and Not I, the *Vav3* cDNA was ligated into the Xho I/Not I–linearized pLVX-IRES-Hyg. A bicistronic lentiviral vector encoding human wild-type Vav3 and green fluorescent protein (GFP) (pCQS1) has been described before (*44*). To generate a lentivirus encoding PyMT (pRL22), we amplified the *PyMT* cDNA from the pBabe-Hygro-PyMT (Addgene) and cloned it into Eco RI/Bam HI–linearized pHIV-ZsGreen (Addgene). The forward and reverse oligonucleotides for the amplification step were 5′-GCGCGCGAATTCATGGATAGAGTTCTGAGC-3′ and 5′-GCGCGCGGATCCCTAGAAATGCCGGGAAC-3′, respectively (restriction sites are underlined). To generate the lentiviral vector encoding a fast cycling form of Rac1 (pMMM1), we amplified the mouse cDNA fragment encoding the mutated Rac1 sequence by PCR with the previously described pMIEG3-Rac1^{F28L} plasmid as template (*45*). Primers were modified to introduce a Xho I site (underlined) at the 5′ end and a Bam HI site (underlined) at the 3′ end in the amplified product. The sequences of the forward and reverse primers were 5′-AGTCCTCGAGATGCAGGCCATCAAGTGTG-3′ and 5′-AGTCGGATCCGCATTTTCTCTTCCTCTTCTTGAC-3′, respectively. The amplified PCR cDNA fragment was digested with the indicated enzymes and cloned into the Xho I/Bam HI–linearized pLVX-IRES-Hyg.

Cell culture

Cells were incubated at 37°C with 5% CO_2. 4T1 cells were cultured in RPMI medium supplemented with 10% fetal calf serum (FCS), penicillin (10 μg/ml), and streptomycin (100 μg/ml). The nonmetastatic 67NR, 4OT7, and 168FARN cell lines were provided by F. Miller (Wayne State University School of Medicine, Detroit, MI) (*24*) and maintained in culture in the aforementioned conditions. Cultures of primary mouse mammary epithelial cells were generated from 8- to 12-week-old wild-type or *Vav2*$^{-/-}$;*Vav3*$^{-/-}$ female mice (FVB background) (*46*), cultured in mammary epithelial cell primary growth medium [Dulbecco's modified Eagle's medium (DMEM)/F12, insulin (5 μg/ml), epidermal growth factor (5 ng/ml), 10% fetal bovine serum (FBS), streptomycin (100 μg/ml), penicillin (100 U/ml), and gentamicin (50 μg/ml)], and transduced in suspension with the pRL22 lentivirus as indicated (*47*). The Lenti-X 293T lentiviral packaging cell line (Clontech) was maintained in DMEM supplemented with 10% tetracycline-free FCS, penicillin (10 μg/ml), and streptomycin (100 μg/ml). To produce lentiviral particles, we transfected the appropriate vector into Lenti-X 293T cells with the Lenti-X HT packaging mix (Clontech). Viral particles were collected 48 hours after transfection and concentrated with the Lenti-X Concentrator Kit (Clontech). Viral titers were determined with the Lenti-X qRT-PCR Titration Kit (Clontech) according to the manufacturer's instructions.

Generation of knockdown cell lines

The shRNA-mediated knockdown of transcripts for *Vav2*, *Vav3*, and the selected Vav family downstream targets was carried out with prepackaged Mission TRC lentiviral particles (Sigma-Aldrich) according to the manufacturer's protocol. The catalog numbers and shRNA sequences yielding the greatest knockdown were TRC0000097094 (5′-CCGGGCCTGCATCTCTGGTTTAGATCTCGAGATCTAAACCAGAGATGCAGGCTTTTTG-3′) for the mouse *Vav2* mRNA; TRC0000097124 (5′-CCGGCCAGCATTTCTCGTCTTAAATCTCGAGATTTAAGACGAGAAATGCTGGTTTTTG-3′) for the mouse *Vav3* mRNA; TRCN0000067219 (5′-CCGGGCCGAGAGATTCAATGAAATTCTCGAGAATTTCATTGAATCTCTCGGCTTTTTG-3′) for the mouse *Itgb6* mRNA; TRCN0000066240 (5′-CCGGCGGGATGAGTTTCTCCTCTATCTCGAGATAGAGGAGAAACTCATCCCGTTTTTG-3′) for the mouse *Itga8* mRNA; TRCN0000022516 (5′-CCGGGCTGACACCAATGCAGTGAATCTCGAGATTCACTGCATTGGTGTCAGCTTTTT-3′) and TRCN0000022515 (5′-CCGGGCACGGATTAATGTGATGAATCTCGAGATTCATCACATTAATCCGTGCTTTTT-3′) for the mouse *Ilk* mRNA (A and B cell clones, respectively); TRCN0000112701 (5′-CCGGGCTCTTCCAAGAACGCTACAACTCGAGTTGTAGCGTTCTTGGAAGAGCTTTTTG-3′) and TRCN0000112700 (5′-CCGGGCTAGATAGCTTGGTTAAGAACTCGAGTTCTTAACCAAGCTATCTAGCTTTTTG-3′) for the mouse *Tacstd2* mRNA (A and B cell clones, respectively); TRCN0000067741 (5′-CCGGGCAAGGTCAACATTTGCTGTACTCGAGTACAGCAAATGTTGACCTTGCTTTTTG-3′) and TRCN0000067738 (5′-CCGGGCTGTCAAGAAGCACATCTTACTCGAGTAAGATGTGCTTCTTGACAGCTTTTTG-3′) for the mouse *Inhba* mRNA (A and B cell clones, respectively); and TRCN0000067938 (5′-CCGGGCACAGGATTTGACCAGTATACTCGAGTATACTGGTCAAATCCTGTGCTTTTTG-3′) and TRCN0000067942 (5′-CCGGCCGTACACATCATTTGAAGAACTC-

GAGTTCTTCAAATGATGTGTACGGTTTTTG-3′) for the mouse *Ptgs2* mRNA (A and B cell clones, respectively). Lentiviral particles containing the empty pLOK.1puro vector (Sigma-Aldrich) were used to generate the control 4T1 cells used in these experiments. Cells were incubated with lentiviral particles in the presence of polybrene (8 μg/ml; Sigma) and selected with puromycin (3 μg/ml; Sigma). The designation and characteristics of the control and knockdown cell lines used in this study are summarized in table S3.

Reexpression of Vav proteins in knockdown 4T1 cell lines

To generate single Vav2– and single Vav3–rescued $KD_{2/3(A)}$ 4T1 cells (see table S3), this knockdown cell clone was infected with lentiviral particles encoding the indicated proteins in the presence of polybrene (8 μg/ml) and then selected with hygromycin (200 μg/ml; Roche). As control, we carried out the same selection procedure with $KD_{2/3(A)}$ 4T1 cells that were infected with lentivirus containing the empty pLVX-IRES-Hyg vector. To generate the rescued $KD_{2/3(A)}$ cell line expressing either wild-type Vav2 plus wild-type Vav3 or $Vav2^{R373A}$ plus wild-type Vav3, *Vav2;Vav3* knockdown cells were first infected with lentiviral particles produced from either the pCCM33 (encoding wild-type HA-tagged Vav2) or the pCCM36 (encoding HA-tagged $Vav2^{R373A}$) vectors and then with lentiviral particles produced from the pCQS1 vector (encoding wild-type, HA-tagged Vav3). Cells were then selected with hygromycin (the hygromycin resistance cassette was in the Vav2-encoding vectors) and subsequently sorted by flow cytometry to isolate GFP-positive cells [which was expressed bicistronically from the same Vav3-encoding pCQS1 vector (*44*)]. The generation of 168FARN cells overexpressing wild-type Vav2 and Vav3 was done following the above protocol. The designation and features of the control and knockdown cell lines used in this study are summarized in table S3.

Analysis of mRNA abundance

Total RNA was extracted from the indicated cells with TRIzol (Sigma), and qRT-PCR was performed with the QuantiTect SYBR Green RT-PCR Kit (Qiagen) and the iCycler machine (Bio-Rad) or, alternatively, the Script One-Step RT-PCR Kit (Bio-Rad) and the StepOnePlus Real-Time PCR System (Applied Biosystems). Raw data were then analyzed with either the iCycler iQ Optical System software (Bio-Rad) or the StepOne software v2.1 (Applied Biosystems). As the normalization control, we used the abundance of the endogenous *P36b4* transcript. Primers used for transcript quantitation were as follows: mouse *Vav2*, 5′-AAGCCTGTGTTGACCTTCCAG-3′ (forward) and 5′-GTGTAATCGATCTCCCGGGAT-3′ (reverse); mouse *Vav3*, 5′-AATAGATCTCCAGCAGTAC-3′ (forward) and 5′-TGGTGTTGAATGGCCCTTG-3′ (reverse); mouse *Itgb6*, 5′-TCACGGCTTCCAGCTTTGGTCT-3′ (forward) and 5′-CTGCACCACCCCAGGCACAG-3′ (reverse); mouse *Itga8*, 5′-TCCTCTGGGCTCCACGGCTC-3′ (forward) and 5′-ACGCAACAGAGACGCGCGAA-3′ (reverse); mouse *Ilk*, 5′-AGGTCGGAAGGGAGGGACCG-3′ (forward) and 5′-GTCCATAGCAGCGTCCCGGC-3′ (reverse); mouse *Tacstd2*, 5′-CACCATGGCGAGGGGCTTGG-3′ (forward) and 5′-CGCCTTGAGCAGCAGGCACT-3′ (reverse); mouse *Inhba*, 5′-GCCGAGTCAGGCACAGCCAG-3′ (forward) and 5′-TTCCTCGGCCTCATCCCCCG-3′ (reverse); mouse *Ptgs2*, 5′-GGGCCCTTCCTCCCGTAGCA-3′ (forward) and 5′-CCATGGCCCAGTCCTCGGGT-3′ (reverse); mouse *Rac1*, 5′-TATGGGACACAGCTGGACAA-3′ (forward) and 5′-ACAGTGGTGTCGCACTTCAG-3′ (reverse); mouse *P36b4*, 5′-TTGATGATGGAGTGTGGCACC-3′ (forward) and 5′-GTGTTTGACAACGGCAGCATT-3′ (reverse).

Immunoblotting and GTPase activity assays

Immunoblots and GST-Pak1 pull-down experiments to determine Rac1 activity in cells were performed as indicated (*48*). Rac1 and RhoA activities were also quantified with the appropriate G-LISA activation kit (Cytoskeleton) according to the manufacturer's specifications (Cytoskeleton).

Animal studies with 4T1 and 168FARN cells

Animal work was done following the protocols approved by the bioethics committees of the University of Salamanca and Consejo Superior de Investigaciones Científicas (CSIC). Female BALB/c mice (6 to 8 weeks old; Charles River) were used for the in vivo studies.

To carry out primary breast cancer tumorigenesis analysis, 5×10^3 viable cells were resuspended in 100 μl of phosphate-buffered saline (PBS) solution and injected orthotopically into the fourth right mammary gland of the recipient mouse. Primary tumor growth was analyzed by measuring tumor length, width, and depth and by calculating tumor volume. Metastatic dissemination of tumor cells was quantified both visually and histologically after sacrificing the mice 35 days after orthotopic implantation.

For direct, long-term lung colonization assays, cells were resuspended in PBS as above and injected into the lateral tail vein (unless otherwise stated, 5×10^4 cells were injected in the experiments). After 2 weeks, mice were euthanized; the chest cavity was exposed through a midline chest incision; the trachea was cannulated with a 20-gauge caterer; and lungs were slowly inflated with 1 ml of India ink (Parker; 1:16 dilution in PBS). Lungs were extracted and destained by immersing in Fekete's solution [100 ml of 70% ethanol (Sigma), 10 ml of 4% formaldehyde (Leica), and 5 ml of 100% glacial acetic acid (Sigma)], and metastatic nodules were counted visually. Alternatively, lungs were extracted, fixed in 4% formaldehyde, and embedded in paraffin for hematoxylin and eosin (H&E) staining. In the case of studies conducted with monocrotaline-treated mice, animals were injected twice intravenously with monocrotaline (1.5 mg/ml; Sigma) the week before the introduction of cancer cells through the tail vein. After 2 weeks, animals were sacrificed and lungs were extracted as described above.

Vascular permeability was evaluated indirectly by measuring the effusion in vivo of a fluorescently labeled dextran from the blood vessels into the primary tumor. For that purpose, a rhodamine-conjugated 70-kD dextran (Invitrogen) was injected intravenously (2 mg per 20 g of body weight) in tumor-bearing mice. One hour later, mice were euthanized; the primary breast tumors were extracted and cut into 30-μm-thick sections, and dextran signals were monitored by confocal microscopy (TCS SP5, Leica). Images were collected with the LAS AF software (Leica), and fluorescence intensities were quantified with the ImageJ software (National Institutes of Health).

To measure the intravasation of cancer cells, we collected ≈1 ml of blood from the heart atrium of tumor-bearing mice, and cells were pelleted by centrifugation. After the elimination of red cells by two lysis cycles in ACK (ammonium-chloride-potassium) buffer (Gibco), we extracted total RNA from the remaining blood cells with TRIzol (Sigma) to quantify the presence of circulating tumor cells through qRT-PCR. This was done by calculating the abundance of the mRNA for the puromycin resistance gene (present exclusively in the 4T1 cells used in this study) in relation to that of an endogenous mouse mRNA (*B2m*). The primers used in these experiments were 5′-GTGTGGGCCCTGTTCCTGCC-3′ (forward viral $Puro^R$ transcript), 5′-GCGCACCGTGGGCTTGTACT-3′ (reverse for viral $Puro^R$ transcript), 5′-ATGGCTCGCTCGGTGACCCT-3′ (forward for *B2m* mRNA), and 5′-CCATTCTCCGGTGGGTGGCG-3′ (reverse for *B2m* mRNA). Values were corrected according to the expression of the viral gene in each cell line when maintained in tissue culture.

To measure the extravasation of breast cancer cells, we labeled the indicated cell lines with 5 μM of a green cell tracker [CellTracker Green CMFDA (carboxymethyl fluorescein diacetate), Invitrogen] for 1 hour and injected them intravenously into mice (1×10^6 cells per mice). After 48 hours, the

mice were injected intravenously with a rhodamine-conjugated lectin (Vector Laboratories) to stain lung capillaries and were sacrificed 60 min later. Lungs were then extracted, fixed in paraformaldehyde, and examined by confocal fluorescence microscopy to visualize the number of cancer cells (green color) present in the lung.

Animal studies with primary breast epithelial cells

Normal, primary breast epithelial cells were obtained from either wild-type or *Vav2*$^{-/-}$;*Vav3*$^{-/-}$ female mice (3 to 12 weeks old; FVB background) as indicated above and, after transduction with the PyMT-encoding pRL22 lentivirus, were reimplanted into the cleared inguinal mammary fat pads of wild-type female mice as described (*47*).

Immunostaining techniques

Immunohistochemical procedures presented in this work were carried out by the personnel of the Molecular Pathology Unit of our Institution. Tissues were extracted, fixed in 4% paraformaldehyde (Sigma), cut into 2- to 3-μm-thick sections, and stained with H&E. For immunohistochemical staining, paraffin-embedded sections were incubated with rabbit polyclonal antibodies to either Ki67 (Novocastra, 1:100 dilution) or CD31 (Abcam, 1:50 dilution). After an overnight incubation, tissue slides were rinsed with PBS, incubated for 1 hour at room temperature in a milk/PBS solution containing a goat anti-rabbit immunoglobulin G–horseradish peroxidase conjugate (GE Healthcare), rinsed with PBS, and developed with diaminobenzidine (Dako). Quantification of signals was done in a blind fashion with the Metamorph-Metaview software (Universal Imaging). Apoptotic cells were detected with the TUNEL-based In Situ Cell Detection Kit (Roche): Sections were deparaffinized, hydrated, and digested with proteinase K (Dako) for 30 min at 37°C and then subjected to the TUNEL reaction according to the manufacturer's instructions; TUNEL-positive cells were visually scored with a standard immunofluorescence microscope (CTR600, Leica).

Determination of in vitro proliferation rates

We used the 3-(4,5-dimethylthiazol-2-yl) 2,5-diphenyltetrazolium bromide (MTT) assay (Sigma) to determine the growth properties of cell lines under study. To this end, cells were plated onto 24-well dishes (7000 cells per well) and cultured in RPMI supplemented with 10% calf serum for the indicated periods. At the indicated time point, the culture medium of each well was discarded and replaced by 250 μl of MTT solution (0.5 mg/ml) in PBS. After 1 hour at 37°C in a 5% CO_2 atmosphere, 500 μl of dimethyl sulfoxide (Sigma) per well was added to dissolve the formazan crystals formed, and the absorbance at the 570-nm wavelength was measured 15 min later with a microplate reader (Ultraevolution, Tecan).

Cell invasion assays

The ability of the cells to invade was assessed with the CytoSelect 24-Well Cell Invasion Assay Kit (Cell Biolabs) according to the manufacturer's protocol. Briefly, 3×10^5 cells in serum-free medium were plated onto the basement membrane layer of the cell culture insert of the invasion chamber. After incubation for 48 hours at 37°C in 5% CO_2, the inserts were stained with Cell Stain Solution (Cell Biolabs) and incubated with Extraction Solution (Cell Biolabs), and the absorbance at the 560-nm wavelength was measured 10 min later with the Ultraevolution microplate reader.

Microarray analyses

All microarray experiments were performed by the personnel of the Genomics and Proteomics Unit of our Institution. Transcriptomal changes were determined with the Mouse Gene 1.0 ST arrays (Affymetrix). Two independent experiments were performed to identify the Vav2/Vav3-dependent transcriptome. In the first, we compared the transcriptomes of control, $KD_{2/3(A)}$, and $KD_{2/3(B)}$ cells (table S3) to identify Vav family–dependent genes. In the second, we compared the transcriptomes of $KD_{2/3(A)}$, $KD_{2/3} + V_2$, $KD_{2/3} + V_3$, and $KD_{2/3} + V_2 + V_3$ cells (table S3). In all cases, total cellular RNA was extracted from three independent exponential cultures of the appropriate cell lines with the RNeasy kit (Qiagen), quantified with 6000 Nano Chips (Agilent Technologies), and used (2.3 μg per sample) to generate labeled complementary RNA probes according to the manufacturer's instructions (Affymetrix). Upon microarray hybridization, raw data were normalized, filtered, and analyzed with the Bioconductor software (http://www.bioconductor.org) with the *Affy* and *Siggenes* applications. To graphically present microarray data, we performed hierarchical clustering analysis with the Bioconductor HCLUST tool. Details about these procedures can be found elsewhere (*49*, *50*).

Criteria for selecting Vav-dependent target genes for functional characterization

We used a number of sieving criteria to select the Vav targets to be knocked down in parental 4T1 cells with shRNA-based strategies. First, we decided to focus only on mRNAs showing reduced abundance in *Vav2;Vav3*-deficient cells because it would be easier to attenuate the prometastatic program of 4T1 cells by eliminating single proteins with positive roles in this process rather than overexpressing single negative metastatic regulators. Likewise, from a clinical and therapeutic point of view, it is easier to treat patients with drug inhibitors rather than by gain-of-function approaches. Keeping in mind this clinically oriented view, we also decided to select mRNAs encoding products potentially amenable to either chemical (for example, enzymes) or antibody-based (for example, surface molecules) inhibitory strategies. Furthermore, we favored genes encoding proteins whose inhibition could have a major impact on the biology of metastatic cancer cells because of their enzymatic, adaptor, or signaling properties. We also took into consideration additional empirical criteria for selecting those targets. Thus, we were interested on selecting targets displaying (i) high fold change variations between the control and double *Vav2;Vav3*-deficient 4T1 cells; (ii) homogeneous behavior in the two independent clones of *Vav2;Vav3*-deficient 4T1 cells; (iii) similar variations in vivo when using microarray-independent techniques (such as by qRT-PCR); and (iv) similar abundance changes in cultured cells and in the tumors derived from them in recipient mice. Some of the genes initially selected for analysis did not fulfill some of the latter criteria. For example, *Igfr2*, *PIP5K1a*, *Plau*, or *Mns* did not pass the third criterion. Likewise, *Adamsts1*, *Gadd45b*, and *Bgalt6* did not fulfill the fourth criterion (they were deregulated in cultured *Vav2;Vav3*-deficient cells but not in primary tumors derived from them). After all those verification steps, we selected six putative target genes (*Itgb6*, *Itga8*, *Ilk*, *Tacstd2*, *Inhba*, and *Ptgs2*) for further characterization in the present work.

Calculation of the percentage of common, synergistic, and Vav family member–specific transcripts in the Vav family–dependent transcriptome of breast cancer cells

These transcriptomal subsets were calculated by Pavlidis template matching (PTM) analysis (*51*) from the microarray data obtained from $KD_{2/3(A)}$, $KD_{2/3(B)}$, $KD_{2/3} + V_2$, $KD_{2/3} + V_3$, and $KD_{2/3} + V_2 + V_3$ cells, with a Q threshold significance cutoff value of ≤0.0025. Control samples were included in the heat maps of each cluster after the statistical analysis.

Overlapping analysis with human cancer microarray studies

The Oncomine/Compendia Bioscience database (*41*) was used to search for general overlaps between the Vav2/Vav3-dependent transcriptome and clinical data from human breast cancer data sets. The microarray data obtained in our two independent experiments [control compared to $KD_{2/3(A)}$ and $KD_{2/3(B)}$; $KD_{2/3(A)}$ compared to $KD_{2/3} + V_2/V_3$] were bioinformatically

analyzed side by side to identify transcripts showing consistent and specular changes between those two analyses and that, therefore, could be directly linked to the known metastatic properties of each of those cell lines. Briefly, the abundance of each mRNA was transformed to *z* scores (mean value, 0; SD, 1) in each independent 4T1 cell line experiment data set to allow differential abundance analysis with a unique data set file. We performed PTM analysis in which the Pearson's correlation coefficient is computed among the intensities measured for each transcript and the values of an independent variable. The threshold significance values used in those analyses were Q value ≤0.0025 and Pearson coefficient either ≥0.82 (in the case of transcripts whose abundance was increased in reconstituted $KD_{2/3} + V_2/V_3$ and control cells) or ≤−0.82 (in the case of transcripts showing reduced abundance in reconstituted $KD_{2/3} + V_2/V_3$ and control cells).

The mouse Probe IDs for the identify transcripts in the above analyses were then humanized with the AILUN web tool (http://ailun.stanford.edu/) (*52*) and loaded onto the Oncomine/Compendia database. Association of the mapped Vav2/Vav3 signature with clinical parameters was tested with Fisher's exact test and was considered significant for odds ratio ≥1.5 and P value ≤0.0001. Overlapping mRNAs with the Loi (*53*) and NKI (*33*) data sets were used to stratify the patients. The sum of the abundance of the mRNAs that were induced both in the Vav2/Vav3 signature and in metastatic human breast tumors was obtained and subtracted with the sum of the abundance values of mRNA repressed in the Vav2/Vav3 signature and metastatic human breast tumors. The value obtained (Vav/Vav3-dependent signature score) was used to divide the patients into high-score and low-score groups, and survival probabilities were obtained for each patient group.

Development of a prognostic Vav2/Vav3 gene signature for lung-specific metastasis in breast cancer patients

Raw microarray data from the Wang data set (*32*) (GEO identifier GSE2034; $n = 286$ patients) were obtained, and signal intensity values were generated with the RMAExpress software (http://rmaexpress.bmbolstad.com). The censored lung metastasis at 5 years as end point from that data set was then used to perform a Cox regression proportional hazard analysis with the humanized Vav2/Vav3 mRNA signature described above. This analysis yields a Cox coefficient (which gives values above or below 0 if the abundance of an mRNA is increased or decreased in metastatic tissue, respectively) and, in addition, performs a Wald test (*54*, *55*) to check the null hypothesis of the Cox coefficient being 0. This analysis resulted in the identification of a minimal Vav2/Vav3 lung metastasis signature (hereinafter referred to as V2/V3LMS) composed of 120 probe sets representing 102 independent mRNAs with significant Cox values ($P \leq 0.05$). Seventy-six (with increase abundance in $KD_{2/3} + V_2/V_3$ cells) and 26 (in decreased abundance in $KD_{2/3} + V_2/V_3$ cells) of those probe sets displayed Cox coefficients above and below 0, respectively (table S7).

To test the prognostic value of the V2/V3LMS, we calculated the V2/V3LMS risk score using the data from each of the patients present in the NKI ($n = 295$) (*33*) and MSKCC ($n = 83$) (*34*) data sets. In the case of the MSKCC data set (generated using Affymetrix HG-U133A arrays), we used the gene $\log_2$ expression values (x_i) and Wald statistics (s_i) with the following formula:

$$\text{V2/V3LMS risk score} = \sum_{i=1}^{120} s_i x_i$$

In the case of the NKI data set (generated using the Agilent array platform), the mean for the s_i values associated with different Affymetrix probe sets of each mRNA was first determined so that only a single s_i value was assigned for transcripts in the Agilent array that had more than one probe set in the Affymetrix Mouse Gene 1.0 ST arrays. The risk score for each patient was then calculated on the basis of the abundance values of V2/V3LMS mRNAs (with the exception of six of them, which were not present in the Agilent arrays: *AQP1*, *C14orf159*, *CCDC21*, *ELOVL1*, *RBM34*, and *TINAGL1*). Risk values were used to subdivide patients into high-risk (percentile 33) and low-risk (percentiles 66 and 100) subsets; subsequently, a Kaplan-Meier analysis was performed with lung-specific (in the case of the NKI and MSKCC data sets) or bone-specific metastasis (in the case of the MSKCC data set) as the final end point.

The comparison of the predictive value of the V2/V3LMS with previously described mRNA signatures (*33*, *34*) was done as indicated above.

Statistics

Depending on the type of experiment, data were analyzed with either the Student's t test or the Mann-Whitney test. Values are given as means ± SEM. P values of ≤0.05, 0.01, and 0.001 were indicated by *, **, and *** in all figures, respectively. Unless otherwise stated, n refers to independent experiments, each performed in triplicate.

SUPPLEMENTARY MATERIALS

www.sciencesignaling.org/cgi/content/full/5/244/ra71/DC1

Fig. S1. Human tumors show differential abundance of Rho GEF transcripts.
Fig. S2. Abundance of Vav family mRNAs and proteins in cell lines used in this study.
Fig. S3. Vav proteins control a large transcriptomal program in breast cancer cells.
Fig. S4. Regulation of the breast cancer cell transcriptome by Vav proteins.
Fig. S5. Vav proteins control the breast cancer cell transcriptome through common, synergistic, and Vav family member–specific routes.
Fig. S6. Generation of knockdown cell lines for Vav family–dependent targets.
Fig. S7. Vav-dependent mRNA signatures have prognostic value in breast cancer.
Table S1. Differential abundance of Rho GEFs in human breast cancer subtypes.
Table S2. Abundance of *Vav2* and *Vav3* mRNAs in the breast cancer luminal A and B subtypes.
Table S3. Cell lines used in this study.
Table S4. Metastasis of 4T1 knockdown cell clones in recipient mice.
Table S5. Transcriptomal changes in 4T1 cells lacking Vav2 and Vav3 (Excel).
Table S6. The Vav2/Vav3-dependent transcriptome associated to the metastatic potential of the 4T1 cells used in this study (Excel).
Table S7. Overexpressed and repressed genes from table S5 associated with human cancer clinical outcome (Excel).
Table S8. Genes belonging to the Vav2/Vav3 lung metastasis signature (Excel).

REFERENCES AND NOTES

1. D. Vigil, J. Cherfils, K. L. Rossman, C. J. Der, Ras superfamily GEFs and GAPs: Validated and tractable targets for cancer therapy? *Nat. Rev. Cancer* **10**, 842–857 (2010).
2. J. L. Bos, H. Rehmann, A. Wittinghofer, GEFs and GAPs: Critical elements in the control of small G proteins. *Cell* **129**, 865–877 (2007).
3. K. L. Rossman, C. J. Der, J. Sondek, GEF means go: Turning on RHO GTPases with guanine nucleotide-exchange factors. *Nat. Rev. Mol. Cell Biol.* **6**, 167–180 (2005).
4. A. Malliri, R. A. van der Kammen, K. Clark, M. van der Valk, F. Michiels, J. G. Collard, Mice deficient in the Rac activator Tiam1 are resistant to Ras-induced skin tumours. *Nature* **417**, 867–871 (2002).
5. K. H. Chang, A. Sanchez-Aguilera, S. Shen, A. Sengupta, M. N. Madhu, A. M. Ficker, S. K. Dunn, A. M. Kuenzi, J. L. Arnett, R. A. Santho, X. Agirre, J. P. Perentesis, M. W. Deininger, Y. Zheng, X. R. Bustelo, D. A. Williams, J. A. Cancelas, Vav3 collaborates with p190-BCR-ABL in lymphoid progenitor leukemogenesis, proliferation and survival. *Blood*, **120**, 800–811 (2012).
6. A. Malliri, T. P. Rygiel, R. A. van der Kammen, J. Y. Song, R. Engers, A. F. Hurlstone, H. Clevers, J. G. Collard, The Rac activator *Tiam1* is a Wnt-responsive gene that modifies intestinal tumor development. *J. Biol. Chem.* **281**, 543–548 (2006).
7. Y. Kawasaki, S. Tsuji, K. Muroya, S. Furukawa, Y. Shibata, M. Okuno, S. Ohwada, T. Akiyama, The adenomatous polyposis coli-associated exchange factors Asef and Asef2 are required for adenoma formation in $Apc^{Min/+}$ mice. *EMBO Rep.* **10**, 1355–1362 (2009).
8. M. S. Sosa, C. Lopez-Haber, C. Yang, H. Wang, M. A. Lemmon, J. M. Busillo, J. Luo, J. L. Benovic, A. Klein-Szanto, H. Yagi, J. S. Gutkind, R. E. Parsons, M. G. Kazanietz, Identification of the Rac-GEF P-Rex1 as an essential mediator of Erbb signaling in breast cancer. *Mol. Cell* **40**, 877–892 (2010).

9. B. Fine, C. Hodakoski, S. Koujak, T. Su, L. H. Saal, M. Maurer, B. Hopkins, M. Keniry, M. L. Sulis, S. Mense, H. Hibshoosh, R. Parsons, Activation of the PI3K pathway in cancer through inhibition of PTEN by exchange factor P-Rex2a. *Science* **325**, 1261–1265 (2009).
10. E. K. Thomas, J. A. Cancelas, Y. Zheng, D. A. Williams, Rac GTPases as key regulators of p210-BCR-ABL-dependent leukemogenesis. *Leukemia* **22**, 898–904 (2008).
11. K. Uhlenbrock, A. Eberth, U. Herbrand, N. Daryab, P. Stege, F. Meier, P. Friedl, J. G. Collard, M. R. Ahmadian, The RacGEF Tiam1 inhibits migration and invasion of metastatic melanoma via a novel adhesive mechanism. *J. Cell Sci.* **117**, 4863–4871 (2004).
12. C. R. Lindsay, S. Lawn, A. D. Campbell, W. J. Faller, F. Rambow, R. L. Mort, P. Timpson, A. Li, P. Cammareri, R. A. Ridgway, J. P. Morton, B. Doyle, S. Hegarty, M. Rafferty, I. G. Murphy, E. W. McDermott, K. Sheahan, K. Pedone, A. J. Finn, P. A. Groben, N. E. Thomas, H. Hao, C. Carson, J. C. Norman, L. M. Machesky, W. M. Gallagher, I. J. Jackson, L. Van Kempen, F. Beermann, C. Der, L. Larue, H. C. Welch, B. W. Ozanne, O. J. Sansom, P-Rex1 is required for efficient melanoblast migration and melanoma metastasis. *Nat. Commun.* **2**, 555 (2011).
13. K. Zhou, Y. Wang, J. L. Gorski, N. Nomura, J. Collard, G. M. Bokoch, Guanine nucleotide exchange factors regulate specificity of downstream signaling from Rac and Cdc42. *J. Biol. Chem.* **273**, 16782–16786 (1998).
14. R. J. Buchsbaum, B. A. Connolly, L. A. Feig, Interaction of Rac exchange factors Tiam1 and Ras-GRF1 with a scaffold for the p38 mitogen-activated protein kinase cascade. *Mol. Cell. Biol.* **22**, 4073–4085 (2002).
15. R. J. Buchsbaum, B. A. Connolly, L. A. Feig, Regulation of p70 S6 kinase by complex formation between the Rac guanine nucleotide exchange factor (Rac-GEF) Tiam1 and the scaffold spinophilin. *J. Biol. Chem.* **278**, 18833–18841 (2003).
16. A. Saveliev, L. Vanes, O. Ksionda, J. Rapley, S. J. Smerdon, K. Rittinger, V. L. Tybulewicz, Function of the nucleotide exchange activity of Vav1 in T cell development and activation. *Sci. Signal.* **2**, ra83 (2009).
17. M. R. Schiller, A. Blangy, J. Huang, R. E. Mains, B. A. Eipper, Induction of lamellipodia by Kalirin does not require its guanine nucleotide exchange factor activity. *Exp. Cell Res.* **307**, 402–417 (2005).
18. M. R. Kuhne, G. Ku, A. Weiss, A guanine nucleotide exchange factor-independent function of Vav1 in transcriptional activation. *J. Biol. Chem.* **275**, 2185–2190 (2000).
19. X. R. Bustelo, Regulatory and signaling properties of the Vav family. *Mol. Cell. Biol.* **20**, 1461–1477 (2000).
20. P. Crespo, K. E. Schuebel, A. A. Ostrom, J. S. Gutkind, X. R. Bustelo, Phosphotyrosine-dependent activation of Rac-1 GDP/GTP exchange by the *vav* proto-oncogene product. *Nature* **385**, 169–172 (1997).
21. K. E. Schuebel, N. Movilla, J. L. Rosa, X. R. Bustelo, Phosphorylation-dependent and constitutive activation of Rho proteins by wild-type and oncogenic Vav-2. *EMBO J.* **17**, 6608–6621 (1998).
22. N. Movilla, X. R. Bustelo, Biological and regulatory properties of Vav-3, a new member of the vav family of oncoproteins. *Mol. Cell. Biol.* **19**, 7870–7885 (1999).
23. J. Baselga, S. M. Swain, Novel anticancer targets: Revisiting Erbb2 and discovering Erbb3. *Nat. Rev. Cancer* **9**, 463–475 (2009).
24. C. J. Aslakson, F. R. Miller, Selective events in the metastatic process defined by analysis of the sequential dissemination of subpopulations of a mouse mammary tumor. *Cancer Res.* **52**, 1399–1405 (1992).
25. R. O. Hynes, Integrins: Bidirectional, allosteric signaling machines. *Cell* **110**, 673–687 (2002).
26. S. A. Wickström, A. Lange, E. Montanez, R. Fässler, The ILK/PINCH/parvin complex: The kinase is dead, long live the pseudokinase! *EMBO J.* **29**, 281–291 (2010).
27. R. Cubas, M. Li, C. Chen, Q. Yao, Trop2: A possible therapeutic target for late stage epithelial carcinomas. *Biochim. Biophys. Acta* **1796**, 309–314 (2009).
28. D. J. Bernard, S. C. Chapman, T. K. Woodruff, Mechanisms of inhibin signal transduction. *Recent Prog. Horm. Res.* **56**, 417–450 (2001).
29. R. J. Flower, The development of COX2 inhibitors. *Nat. Rev. Drug Discov.* **2**, 179–191 (2003).
30. G. P. Gupta, D. X. Nguyen, A. C. Chiang, P. D. Bos, J. Y. Kim, C. Nadal, R. R. Gomis, K. Manova-Todorova, J. Massagué, Mediators of vascular remodelling co-opted for sequential steps in lung metastasis. *Nature* **446**, 765–770 (2007).
31. M. Kido, T. Hirose, K. Tanaka, T. Kurozumi, Y. Shoyama, Increased alveolar-capillary membrane permeability by monocrotaline. *Jpn. J. Med.* **20**, 170–179 (1981).
32. Y. Wang, J. G. Klijn, Y. Zhang, A. M. Sieuwerts, M. P. Look, F. Yang, D. Talantov, M. Timmermans, M. E. Meijer-van Gelder, J. Yu, T. Jatkoe, E. M. Berns, D. Atkins, J. A. Foekens, Gene-expression profiles to predict distant metastasis of lymph-node-negative primary breast cancer. *Lancet* **365**, 671–679 (2005).
33. M. J. van de Vijver, Y. D. He, L. J. van't Veer, H. Dai, A. A. Hart, D. W. Voskuil, G. J. Schreiber, J. L. Peterse, C. Roberts, M. J. Marton, M. Parrish, D. Atsma, A. Witteveen, A. Glas, L. Delahaye, T. van der Velde, H. Bartelink, S. Rodenhuis, E. T. Rutgers, S. H. Friend, R. Bernards, A gene-expression signature as a predictor of survival in breast cancer. *N. Engl. J. Med.* **347**, 1999–2009 (2002).
34. A. J. Minn, G. P. Gupta, P. M. Siegel, P. D. Bos, W. Shu, D. D. Giri, A. Viale, A. B. Olshen, W. L. Gerald, J. Massagué, Genes that mediate breast cancer metastasis to lung. *Nature* **436**, 518–524 (2005).
35. D. X. Nguyen, P. D. Bos, J. Massagué, Metastasis: From dissemination to organ-specific colonization. *Nat. Rev. Cancer* **9**, 274–284 (2009).
36. J. M. Carvajal-Gonzalez, S. Mulero-Navarro, A. C. Roman, V. Sauzeau, J. M. Merino, X. R. Bustelo, P. M. Fernandez-Salguero, The dioxin receptor regulates the constitutive expression of the *vav3* proto-oncogene and modulates cell shape and adhesion. *Mol. Biol. Cell* **20**, 1715–1727 (2009).
37. V. Sauzeau, J. M. Carvajal-González, A. S. Riolobos, M. A. Sevilla, M. Menacho-Márquez, A. C. Román, A. Abad, M. J. Montero, P. Fernández-Salguero, X. R. Bustelo, Transcriptional factor aryl hydrocarbon receptor (Ahr) controls cardiovascular and respiratory functions by regulating the expression of the *Vav3* proto-oncogene. *J. Biol. Chem.* **286**, 2896–2909 (2011).
38. G. P. Gupta, J. Massagué, Cancer metastasis: Building a framework. *Cell* **127**, 679–695 (2006).
39. S. Valastyan, R. A. Weinberg, Tumor metastasis: Molecular insights and evolving paradigms. *Cell* **147**, 275–292 (2011).
40. E. F. Solomayer, I. J. Diel, G. C. Meyberg, C. Gollan, G. Bastert, Metastatic breast cancer: Clinical course, prognosis and therapy related to the first site of metastasis. *Breast Cancer Res. Treat.* **59**, 271–278 (2000).
41. D. R. Rhodes, S. Kalyana-Sundaram, V. Mahavisno, R. Varambally, J. Yu, B. B. Briggs, T. R. Barrette, M. J. Anstet, C. Kincead-Beal, P. Kulkarni, S. Varambally, D. Ghosh, A. M. Chinnaiyan, Oncomine 3.0: Genes, pathways, and networks in a collection of 18,000+ cancer gene expression profiles. *Neoplasia* **9**, 166–180 (2007).
42. C. Hatzis, L. Pusztai, V. Valero, D. J. Booser, L. Esserman, A. Lluch, T. Vidaurre, F. Holmes, E. Souchon, H. Wang, M. Martin, J. Cotrina, H. Gomez, R. Hubbard, J. I. Chacón, J. Ferrer-Lozano, R. Dyer, M. Buxton, Y. Gong, Y. Wu, N. Ibrahim, E. Andreopoulou, N. T. Ueno, K. Hunt, W. Yang, A. Nazario, A. DeMichele, J. O'Shaughnessy, G. N. Hortobagyi, W. F. Symmans, A genomic predictor of response and survival following taxane-anthracycline chemotherapy for invasive breast cancer. *JAMA* **305**, 1873–1881 (2011).
43. L. Rodrigues, M. Pires de Miranda, M. J. Caloca, X. R. Bustelo, J. P. Simas, Activation of Vav by the gammaherpesvirus M2 protein contributes to the establishment of viral latency in B lymphocytes. *J. Virol.* **80**, 6123–6135 (2006).
44. C. Quevedo, V. Sauzeau, M. Menacho-Márquez, A. Castro-Castro, X. R. Bustelo, Vav3-deficient mice exhibit a transient delay in cerebellar development. *Mol. Biol. Cell* **21**, 1125–1139 (2010).
45. F. Guo, Y. Zheng, Rho family GTPases cooperate with *p53* deletion to promote primary mouse embryonic fibroblast cell invasion. *Oncogene* **23**, 5577–5585 (2004).
46. V. Sauzeau, M. Jerkic, J. M. López-Novoa, X. R. Bustelo, Loss of *Vav2* proto-oncogene causes tachycardia and cardiovascular disease in mice. *Mol. Biol. Cell* **18**, 943–952 (2007).
47. R. M. Larive, A. Abad, C. M. Cardaba, T. Hernández, M. Cañamero, E. de Álava, E. Santos, B. Alarcón, X. R. Bustelo, The Ras-like protein R-Ras2/TC21 is important for proper mammary gland development. *Mol. Biol. Cell* **23**, 2373–2387 (2012).
48. A. Castro-Castro, V. Ojeda, M. Barreira, V. Sauzeau, I. Navarro-Lérida, O. Muriel, J. R. Couceiro, F. X. Pimentel-Muiños, M. A. Del Pozo, X. R. Bustelo, Coronin 1A promotes a cytoskeletal-based feedback loop that facilitates Rac1 translocation and activation. *EMBO J.* **30**, 3913–3927 (2011).
49. I. M. Berenjeno, F. Núñez, X. R. Bustelo, Transcriptomal profiling of the cellular transformation induced by Rho subfamily GTPases. *Oncogene* **26**, 4295–4305 (2007).
50. I. M. Berenjeno, X. R. Bustelo, Identification of the Rock-dependent transcriptome in rodent fibroblasts. *Clin. Transl. Oncol.* **10**, 726–738 (2008).
51. P. Pavlidis, W. S. Noble, Analysis of strain and regional variation in gene expression in mouse brain. *Genome Biol.* **2**, RESEARCH0042 (2001).
52. R. Chen, L. Li, A. J. Butte, AILUN: Reannotating gene expression data automatically. *Nat. Methods* **4**, 879 (2007).
53. S. Loi, B. Haibe-Kains, C. Desmedt, P. Wirapati, F. Lallemand, A. M. Tutt, C. Gillet, P. Ellis, K. Ryder, J. F. Reid, M. G. Daidone, M. A. Pierotti, E. M. Berns, M. P. Jansen, J. A. Foekens, M. Delorenzi, G. Bontempi, M. J. Piccart, C. Sotiriou, Predicting prognosis using molecular profiling in estrogen receptor-positive breast cancer treated with tamoxifen. *BMC Genomics* **9**, 239 (2008).
54. S. D. Silvey, The Lagrangian multiplier test. *Ann. Math. Stat.* **30**, 389–407 (1959).
55. A. Wald, Tests of statistical hypotheses concerning several parameters when the number of observations is large. *Trans. Am. Math. Soc.* **54**, 426–482 (1943).

Acknowledgments: We thank the personnel of the Genomics and Proteomics, Bioinformatics, Molecular Pathology, and Microscopy units of our Center for their expert technical help; A. Abad and M. Blázquez for technical laboratory work; M. Dosil for comments on the manuscript; and F. Miller for providing the 67NR, 168FARN, and 4TO7 cells. **Funding:** X.R.B.'s work was supported by the Spanish Ministry of Economy and Competitiveness (SAF2009-07172 and RD06/0020/0001), the Castilla-León Autonomous Government (GR97), the 7th Framework European Union Program (FP7-HEALTH-2007-A-201862), and the Spanish Association Against Cancer. A portion of X.R.B.'s funding comes from the European Regional Development Fund. Work in J.M.P.'s laboratory is partially supported by grants from the Spanish Ministry of Economy and Competitiveness (SAF2006-00121 and

RD06/0020/0029) and the Madrid Autonomous Government (S2006/BIO-0232). C.C.'s and M.M.-M.'s salaries were partially supported by the JAE-Doc program, the Spanish National Research Council, the RD06/0020/0001 grant, and the European Regional Development Fund. **Author contributions:** C.C. and M.M.-M. performed the experiments shown in Figs. 1, 3 (A to F), 4 (C to G), 5 (A and B), 6, and 7; figs. S2, S3 (B to D), S4 (A and F), and S6; and table S4. C.C. generated most of the cell lines, generated the raw microarray data, and carried out the experiments shown in table S5 and Figs. 2, 3G, 4 (H and I), and 5 (C to J). M.M.-M. generated some of the reconstituted cell lines used in the work and carried out the experiments shown in fig. S4 (B to I). R.G.-E. and J.M.P. carried out the metagenomic experiments shown in table S2 and the bioinformatics analysis presented in figs. S3A and S5 to S7 as well as in tables S6 to S8. R.M.L. performed the experiments shown in Fig. 4 (A and B). O.B. and F.S.-M. collaborated in the short-term extravasation experiments shown in Fig. 3. Artwork was generated by C.C., M.M.-M., R.G.-E., R.M.L., and X.R.B. and edited by X.R.B. X.R.B. directed the work, carried out the metagenomic analyses shown in fig. S1 and table S1, and wrote the manuscript. **Competing interests:** The authors declare that they have no competing interests. **Data and materials availability:** The microarray data generated in this work have been uploaded at the GEO database (http://www.ncbi.nlm.nih.gov/geo/query/acc.cgi?token=fbefjswiwsqksfu&acc=GSE33348).

Submitted 14 February 2012
Accepted 5 September 2012
Final Publication 2 October 2012
10.1126/scisignal.2002962
Citation: C. Citterio, M. Menacho-Márquez, R. García-Escudero, R. M. Larive, O. Barreiro, F. Sánchez-Madrid, J. M. Paramio, X. R. Bustelo, The Rho exchange factors Vav2 and Vav3 control a lung metastasis–specific transcriptional program in breast cancer cells. *Sci. Signal.* **5**, ra71 (2012).

Science Signaling

The Rho Exchange Factors Vav2 and Vav3 Control a Lung Metastasis–Specific Transcriptional Program in Breast Cancer Cells

Carmen Citterio, Mauricio Menacho-Márquez, Ramón García-Escudero, Romain M. Larive, Olga Barreiro, Francisco Sánchez-Madrid, Jesús M. Paramio and Xosé R. Bustelo

Sci. Signal. **5** (244), ra71.
DOI: 10.1126/scisignal.2002962

Metastatic Route to the Lung

Many individuals with cancer die from secondary tumors or metastases that spread through blood or lymph vessels to other tissues from the primary tumor site. The members of the Rho family of guanosine triphosphatases (GTPases) promote tumor growth and metastasis and are activated by guanine nucleotide exchange factors (GEFs). Rho GEFs are attractive pharmacological targets because they have potentially druggable catalytic activities and more restricted distribution patterns than Rho proteins. Citterio *et al.* found that the mRNA abundance of the GEFs Vav2 and Vav3 was increased in certain breast cancer subtypes in patient samples. Mice implanted with breast cancer cells in which Vav2 and Vav3 had been silenced developed slowly growing breast tumors and did not develop lung metastases. Vav2- and Vav3-deficient breast cancer cells showed an altered transcriptional profile, leading the authors to further analyze the role of select target genes encoding proteins that could be pharmacologically inhibited, such as the enzyme cyclooxygenase-2. When implanted into mice, breast cancer cells with deficiencies in individual Vav target genes showed defects in proliferation, angiogenesis, the ability to enter or exit blood vessels during metastasis, and the ability to colonize the lung. When applied to human breast cancer data sets, the changes in the abundance of a subset of mRNAs from the Vav transcriptome generated a gene signature that accurately predicted if patients survived and were free of detectable lung metastasis. These results identify possible targets for treating breast cancer and preventing secondary lung metastases and provide a potential prognostic tool for clinicians.

Science Signaling (ISSN 1937-9145) is published by the American Association for the Advancement of Science, 1200 New York Avenue NW, Washington, DC 20005. The title *Science Signaling* is a registered trademark of AAAS.